

# Unbiased Expression Mapping Identifies a Link between the Complement and Cholinergic Systems in the Rat Central Nervous System

Rickard P. F. Lindblom,\* Mikael Ström,\* Matthias Heinig,<sup>†,‡</sup> Faiez Al Nimer,\*  
Shahin Aeinehband,\* Alexander Berg,<sup>§</sup> Cecilia A. Dominguez,\* Swetha Vijayaraghavan,<sup>¶</sup>  
Xing-Mei Zhang,\* Karin Harnesk,\* Johan Zelano,<sup>§</sup> Norbert Hübner,<sup>†</sup> Staffan Cullheim,<sup>§</sup>  
Taher Darreh-Shori,<sup>¶</sup> Margarita Diez,\* and Fredrik Piehl\*

The complement system is activated in a wide spectrum of CNS diseases and is suggested to play a role in degenerative phenomena such as elimination of synaptic terminals. Still, little is known of mechanisms regulating complement activation in the CNS. Loss of synaptic terminals in the spinal cord after an experimental nerve injury is increased in the inbred DA strain compared with the PVG strain and is associated with expression of the upstream complement components C1q and C3, in the absence of membrane attack complex activation and neutrophil infiltration. To further dissect pathways regulating complement expression, we performed genome-wide expression profiling and linkage analysis in a large F<sub>2</sub>(DA × PVG) intercross, which identified quantitative trait loci regulating expression of C1qa, C1qb, C3, and C9. Unlike C1qa, C1qb, and C9, which all displayed distinct coregulation with different *cis*-regulated C-type lectins, C3 was regulated in a coexpression network immediately downstream of butyrylcholinesterase. Butyrylcholinesterase hydrolyses acetylcholine, which exerts immunoregulatory effects partly through TNF- $\alpha$  pathways. Accordingly, increased C3, but not C1q, expression was demonstrated in rat and mouse glia following TNF- $\alpha$  stimulation, which was abrogated in a dose-dependent manner by acetylcholine. These findings demonstrate new pathways regulating CNS complement expression using unbiased mapping in an experimental *in vivo* system. A direct link between cholinergic activity and complement activation is supported by *in vitro* experiments. The identification of distinct pathways subjected to regulation by naturally occurring genetic variability is of relevance for the understanding of disease mechanisms in neurologic conditions characterized by neuronal injury and complement activation. *The Journal of Immunology*, 2014, 192: 1138–1153.

**T**he complement system has important and diverse immune functions and is involved in aspects of both health preservation and disease development (1, 2). The system consists of a large number of proteins that together form an intricate biological network regulated at many levels, where many of the

components have both signaling and direct effector functions (3). Classically, the complement system is counted as a part of the innate immune system, but in various ways it also acts as a bridge between innate and adaptive immune responses (4–6).

In its final step, activation of the complement cascade leads to the assembly of complement subunits C5b–9 to form the membrane attack complex (MAC), which disrupts cell membrane integrity, leading to lysis of the targeted cell. However, there are multiple steps before the formation of the MAC and many of the cleaved complement products are themselves biologically active in functions such as chemotaxis and cell signaling (4). The >60 constituents of the system provide basis for flexibility, but also for complex regulation, and in many settings the initial part of the cascade can be partially activated without formation of the MAC (2, 7).

Complement activation has also been demonstrated in a wide range of CNS diseases, including acute conditions such as trauma (8) and stroke (9), as well as in states of chronic neurodegeneration (10–13). However, despite the well-established role of complement in CNS pathology, there is still limited knowledge of how complement activation is regulated in the CNS. In a previous transcriptional profiling study in the inbred rat strains Dark Agouti (DA) and Piebald Virol Glaxo (PVG), expression of both C1q and C3 displayed injury- and strain-dependent regulation after ventral root avulsion (VRA), a reproducible model of proximal nerve injury, and was associated with the extent of axotomy-induced nerve cell loss (14). Additionally, C1qb expression correlated with nerve cell loss in an advanced intercross line, providing a genetic link between local expression of complement molecules and axotomy-induced neurodegeneration (14).

\*Neuroimmunology Unit, Department of Clinical Neuroscience, Karolinska Institutet, 171 77 Stockholm, Sweden; <sup>†</sup>Max Delbrück Center for Molecular Medicine, 13125 Berlin, Germany; <sup>‡</sup>Max Planck Institute for Molecular Genetics, 14195 Berlin, Germany; <sup>§</sup>Division of Neuronal Regeneration, Department of Neuroscience, Karolinska Institutet, 171 77 Stockholm, Sweden; and <sup>¶</sup>Department of Neurobiology, Care Sciences and Society, Alzheimer Neurobiology Center, Karolinska Institutet, 171 77 Stockholm, Sweden

Received for publication May 22, 2013. Accepted for publication November 18, 2013.

This work was supported by the Sixth Framework Program of the European Union Grants LSHM-CT-2005-018637 (NeuroproMiSe) and LSHG-CT-2005019015 (EURATools), the Seventh Framework Program of the European Union Grant HEALTH-F4-2010-24150 (EURATrans), the Swedish Research Council, the Swedish Brain Foundation, the King Gustaf V's 80 Years Foundation, and the Swedish Association of Persons with Neurological Disabilities. The funders had no role in study design, data collection and analysis, decision to publish, or preparation of the manuscript.

Address correspondence and reprint requests to Dr. Rickard P.F. Lindblom, Karolinska University Hospital, Center for Molecular Medicine L8:04, 171 76 Stockholm, Sweden. E-mail address: rickard.lindblom@ki.se

The online version of this article contains supplemental material.

Abbreviations used in this article: ACh, acetylcholine; AChE, acetylcholinesterase; BChE, butyrylcholinesterase; CLEC, C-type lectin; DA, Dark Agouti; eQTL, expression quantitative trait loci; KLR, killer cell lectin-like receptor; MAC, membrane attack complex; Mb, megabase; MPO, myeloperoxidase; PVG, Piebald Virol Glaxo; TBI, traumatic brain injury; TF, transcription factor; TFBS, transcription factor binding site; VRA, ventral root avulsion; vWF, von Willebrand factor.

Copyright © 2014 by The American Association of Immunologists, Inc. 0022-1767/14/\$16.00

We here carried out a detailed, large-scale, genome-wide expression quantitative trait loci (eQTL) mapping in an F<sub>2</sub>(DA × PVG) intercross demonstrating linkage of locally expressed complement components to different *cis*-regulated members of the C-type lectin (CLEC) family. We also identified a gene expression network where the key complement component C3 was regulated downstream of butyrylcholinesterase (BChE), an enzyme that degrades acetylcholine (ACh), thus suggesting a link between cholinergic signaling and complement activation, which was confirmed functionally *in vitro*.

## Materials and Methods

### Animals and surgery

The DA.RT1<sup>av1</sup>, hereafter called DA, strain was originally obtained from Prof. Hans Hedrich (Medizinische Hochschule, Hannover, Germany), whereas the PVG.RT1<sup>av1</sup> strain, hereafter called PVG, is an MHC congenic strain originating from Harlan U.K. (Blackthorn, U.K.). The animals were bred at our in-house animal facility under pathogen-free and climate-controlled conditions with 12 h light/dark cycles. They were housed in polystyrene cages with wood shavings and provided with a standard rodent diet and water ad libitum.

To generate an F<sub>2</sub> intercross population, breeding couples composed of both DA and PVG male and female rats, respectively, were set up to generate two groups of offspring (F<sub>1</sub>). These two groups were subsequently mated reciprocally to generate four groups of F<sub>2</sub> progeny. Both female and male rats were included, and a total of 144 F<sub>2</sub> animals were used for the microarray study with 5 d postoperative survival with dissection of the ipsilateral ventral quadrant of the L4 segment.

Apart from the F<sub>2</sub> cohort, a separate kinetic study including 72 DA and PVG animals was performed. All animals except for naive controls were subjected to a unilateral avulsion of the left L3–L5 ventral roots, as previously described (15), at an age of 9–12 wk. In short, a dorsal laminectomy was performed at the level of the L2–L3 vertebrae. The dura was delicately opened with the point of a needle, and by gently moving the sensory nerve roots the L3–L5 ventral roots were identified and avulsed from the spinal cord using microforceps. The muscles and skin were then sutured in layers. Postoperative analgesia (buprenorphine, 0.1 ml, 0.3 mg/ml; RB Pharmaceuticals, Slough, England) was given *s.c.* twice daily for 3 d. The rats in the kinetic study were divided into groups of five to seven animals, including an unoperated control group and five experimental groups with 1, 3, 5, 7, or 14 d postoperative survival. Five days postoperative survival (*n* = 9) was used for perfused material for immunohistochemistry. Traumatic brain injury (TBI) was performed as a controlled-contusion weight drop injury (*n* = 10) as previously described (16). All animal experiments in the study were approved (N42/06, N32/09, N122/11, and N365/08) by the local Ethical Committee for Animal Experimentation (Stockholms Norra Djurförsöksetiska Nämnd).

### Genotyping

Genomic DNA was extracted from rat tail tips as previously described (17). Polymorphic microsatellite markers were selected from the Rat Genome Database (<http://rgd.mcw.edu>) and the Ensembl database (<http://www.ensembl.org>). The F<sub>2</sub> intercross was genotyped with 113 microsatellite

markers evenly distributed across the genome, with an average distance of 20 cM based on previous knowledge of optimum spacing (18). The successful genotyping rate was 95.3%. Both fluorescent and radioactive genotyping methods were used. Fluorophore-conjugated primers were purchased from Applied Biosystems (Carlsbad, CA) or Eurofins MWG Operon (Ebersberg, Germany). PCR amplifications were performed using a standard protocol, and PCR products were separated using an electrophoresis capillary sequencer (ABI3730) and analyzed with GeneMapper v3.7 software (Applied Biosystems). Radioactive PCR amplification was performed as previously described (19) with [ $\gamma$ -<sup>32</sup>P]ATP end-labeled forward primers (Prologo, now part of Sigma-Aldrich, St. Louis, MO). The PCR products were size-fractionated on 6% polyacrylamide gels and visualized by autoradiography. All genotypes were evaluated manually by two independent observers.

### RT-PCR

RNA preparation from spinal cord tissue and RT-PCR was performed according to a standard protocol. Spinal cord samples were dissociated in Lysing Matrix D tubes (MP Biomedicals, Irvine, CA) on a FastPrep homogenizer (MP Biomedicals, Solon, OH) and resuspended in RLT buffer (Qiagen, Hilden, Germany) for total RNA preparation. Cells were lysed directly in RLT buffer. Total RNA was extracted, purified, and on the column DNase I treated using an RNeasy Mini kit (Qiagen) and RNase-free DNase set (Qiagen), according to the manufacturer's protocols. RNA from the L3 segments was further processed for cDNA preparation by reverse transcription with 10  $\mu$ l total RNA using iScript (Bio-Rad, Hercules, CA), and RNA from the L4 segments was taken for array hybridization, as described below. All steps were performed under RNase-free conditions. Real-time PCR was conducted using a three-step PCR protocol using iQ5 or Bio-Rad CFX 384 SYBR Green optical system software (Bio-Rad). All primers and probes were designed with Beacon Designer 5.0 software (Bio-Rad) and tested for specificity by running the amplified product on gels with silver staining. Two housekeeping genes (hypoxanthine-guanine phosphoribosyltransferase and GAPDH) were used to normalize the levels of mRNA expression of the studied transcripts, and normalized expression levels were calculated with the iQ5 or CFX 384 software (Bio-Rad). We chose to use C1qb as a marker for C1q expression because it was represented on the RG-U34A chips used in our previous microarray study and shown to correlate with nerve cell loss in an advanced intercross line (14). The C1q molecule is an oligomer formed by six C1qa, six C1qb, and six C1qc molecules (20). Two different primer pairs were used to confirm expression of the gene orthologous to human transcription factor FOXK2 (gene ID ENSR-NOG00000039894, <http://www.ensembl.org>). See Table I for primer sequences.

### Immunohistochemistry

Spinal cord sections were serially cut (14  $\mu$ m) on a cryostat (Leica Microsystems, Wetzlar, Germany) at the level of L4 segment, or L3 segment in the case of the paraformaldehyde-perfused animals used for synaptophysin, C3, and BChE stainings. Brain sections were cut at a distance of 1800  $\mu$ m around the epicenter of the injury. Sections were thawed onto Superfrost Plus microscope slides (Menzel-Gläser, Braunschweig, Germany) and stored at  $-20^{\circ}\text{C}$  until further processing for immunohistochemistry or *in situ* hybridization. Sections were postfixed in 4% formaldehyde and 0.4% picric acid in 0.16 M phosphate buffer (pH 7.2) for

Table I. Sequences of primers used for RT-PCR

Primer Name	Forward Sequence (5'→3')	Reverse Sequence (5'→3')
<b>Rats</b>		
Gapdh	TCAACTACATGGTCTACATGTTCCAG	TCCCATTTCTCAGCCTTGACTG
Hprt	CTCATGGACTGATTATGGACAGGAC	GCAGGTCAGCAAAGAACTTATAGCC
C1qb	TCATAGAACACGAGGATTCCATACA	GACCCAGTACAGCTGCCTTTGG
C3	GGGAGCCCCATGTACTCCAT	GGGACGTACCCCTGAGCAT
BChE	TTCTACTATGTGGACTGGTTAGGTG	GACTTCTGTGTCTCAAGGTTAGG
CD59	CCAGGCGGACTTGTGTAAC	ACCGAGGTCACCAGCAAC
FOXK2 ortholog primer 1	CATTACAGCCCTATCCAGAGAG	TAGCCCTTGTCCGCAGTCC
FOXK2 ortholog primer 2	ATAACATTACAGCCCTATCCAGAG	TAGCCCTTGTCCGCAGTCC
Foxk2	CCCGTGTGATACCACTGACCTC	CCTTGTCCGCAGTCCCTAGTATG
<b>Mice</b>		
Gapdh	TCAACTACATGGTCTACATGTTCCAG	TCCCATTTCTCAGCCTTGACTG
Hprt	CTCATGGACTGATTATGGACAGGAC	GCAGGTCAGCAAAGAACTTATAGCC
C1qb	AGAGCAAGAGGAGGTTGTTTAC	GCAGGAAGATGGTGTGGATAGG
C3	GCTGCTGTCTTCAATCACTTCATC	GCCTCTTGCCTCTCTCTATGC
	TCAACTACATGGTCTACATGTTCCAG	TCCCATTTCTCAGCCTTGACTG

2 h at room temperature, rinsed in PBS, and incubated overnight at 4°C with primary antisera directed against synaptophysin (rabbit anti-rat 1:200; Invitrogen, Carlsbad, CA), or postfixed for 30 min in 4% formaldehyde at room temperature before incubation with the following Abs—myeloperoxidase (MPO; rabbit anti-rat, 1:100; Abcam, Cambridge, U.K.), MAC, or C5b-9 (mouse anti-rat, 1:50, Hycult Biotech, Uden, The Netherlands), ILF1 or FoxK2 (rabbit anti-human, 1:200; Abcam), C3 (mouse anti-rat, 1:100; Abbiotec, San Diego, CA), von Willebrand factor (vWF; rabbit anti-human, 1:200; Abcam), BChE (mouse anti-rat, 1:200; the Ab was developed and provided by Dr. Anna Hrabovska (21)—then rinsed in PBS, incubated for 60 min with appropriate fluorophore-conjugated secondary Ab (Cy3 donkey anti-rabbit, 1:500 [Jackson ImmunoResearch Laboratories, West Grove, PA] and Alexa Fluor 488 donkey-anti rabbit, 1:150 and Alexa Fluor 594 goat anti-mouse, 1:300 [both from Invitrogen]), diluted in PBS and 0.3% Triton X-100, and then rinsed in PBS and mounted in PBS-glycerol (1:3). For staining of the MAC, an avidin/biotin complex-kit (Vector Laboratories, Burlingame, CA) was used with visualization using a diaminobenzidine substrate kit from the same manufacturer according to instructions.

#### *Immunohistochemical imaging and quantification of synaptophysin immunoreactivity*

Sections processed for immunohistochemistry were examined in a Zeiss LSM 5 Pascal confocal laser scanning microscope (Carl Zeiss, Göttingen, Germany) or a Leica DM RBE microscope system (Leica). Semiquantitative measurements of synaptophysin immunoreactivity were carried out in ImageJ (National Institutes of Health, Bethesda, MD) on confocal images. The immunoreactivity in the ventral horn of the spinal cord was compared with the corresponding contralateral area in the same spinal cord section. The images were taken in the optical plane with the maximal immunoreactivity, and all settings for compared images were identical. At least four spinal cord sections from each animal were measured and the mean ipsilateral/contralateral signal ratio for each animal was used for statistical analysis.

#### *In situ hybridization*

Unfixed tissue sections were prepared as described above. Forty-eight–mer anti-sense oligonucleotides were synthesized (CyberGene, Huddinge, Sweden) and in situ hybridization was performed as previously described (22). Briefly, the probes were labeled at the 3' end with deoxyadenosine- $\alpha$ -triphosphate [ $^{32}$ P] and hybridized to the sections without pretreatment for 16–18 h at 42°C. The hybridization mixture contained 50% formamide, 4 $\times$  SSC, 1 $\times$  Denhardt's solution, 1% sarcosyl (*N*-lauroylsarcosine; Sigma-Aldrich), 0.02 M phosphate buffer, 10% dextran sulfate (Pharmacia), 250  $\mu$ g/ml yeast tRNA (Sigma-Aldrich), 500  $\mu$ g/ml sheared and heat-denatured salmon sperm DNA (Sigma-Aldrich), and 200 mM DTT (LKB, Bromma, Sweden). Following hybridization, the sections were washed several times in 1 $\times$  SSC at 55°C, dehydrated in ethanol, and dipped in NTB2 nuclear track emulsion (Kodak, Rochester, NY). After 3 wk, the slides were developed in D-19 developer (Kodak), counterstained with toluidine blue, and coverslipped. The sections were examined in a Leica DM RBE microscope equipped with a dark field condenser. Images were captured with a Nikon CoolPix 990 camera (Nikon, Tokyo, Japan). The sequences of the probes were checked in a GenBank database search to exclude significant homology with other genes. The C3 probe is the anti-sense sequence corresponding to nucleotides 3301–3348 of the human C3 gene (23) and for CD59 two probes with the 5'-TTCCGGATACAGCAACAAGACAAGCATCCAGGTTAGGAGAGCAAGTGC-3' and 5'-CGCTGTCTTCCCCAATAGGGAGATTGCCCATTTGGCTTGCTTC-3' were used.

#### *Amplification of RNA and array hybridization*

The microarray analysis was performed at the Bioinformatics and Expression Analysis Core Facility of the Karolinska Institutet using Affymetrix rat gene 1.0 ST array chips (Affymetrix, Santa Clara, CA). Array hybridization and labeling was performed according to a standardized protocol as previously described (24).

#### *eQTL and enrichment analysis*

The microarray data are available in a Minimal Information about a Microarray Experiment-compliant format at the ArrayExpress Database (<http://www.ebi.ac.uk/arrayexpress>) under accession code E-MTAB-303. Microarray gene expression data were normalized using the robust multiarray average algorithm (25), implemented in the Bioconductor package “oligo”. Briefly, raw expression intensities were background corrected, quantile normalized, log<sub>2</sub> transformed, and summarized on probe set level.

On the rat gene ST 1.0 array, genes are represented by multiple probe sets. Affymetrix assigns these probe sets to transcript clusters. We have used average expression values of all probe sets annotated to a transcript cluster to measure expression on the level of a gene based on annotation from Bioconductor package “pd.ragene.1.0.st.v1”.

Subsequently, we mapped eQTL for all transcript clusters using the QTL Reaper software (26) against the 113 genomic markers. To assess genome-wide significance of eQTL we performed 10<sup>6</sup> permutations; a *p* value <0.01 at the genome-wide level was considered significant. We classified eQTL into *cis*- or *trans*-acting according to the distance between the locations of genetic marker and the affected transcript. When the distance was <20 megabases (Mb), we assumed *cis* regulation; otherwise, we assumed *trans* regulation. The identified clusters were analyzed for enrichment of specific pathways and expression patterns using the Bioconductor package GOSTATS (27). To enable identification of strongly connected hub genes in eQTL gene expression networks, we applied a graphical Gaussian model. For each cluster of *trans*-regulated transcripts, we constructed gene expression networks as previously described reporting significant edges with a false discovery rate of <0.1 (28).

#### *Analysis of transcription factor binding site enrichment*

To quantify the effect of differential regulation of the FOXK2 ortholog (Ensembl Gene ID ENSRNOG0000039894) on its targets, we searched for *trans*-eQTL co-occurring at the peak marker of the transcription factor (TF) eQTL as recently described by Heinig et al. (29). In brief, we predicted TF binding affinities to the proximal promoters of all protein coding genes using a biophysical (30) and statistical (31) model based on binding site preferences of FoxK2 in the form of position weight matrices (V\$FOX\_Q2) from the TRANSFAC database (<http://biobase-international.com>). Putative promoter sequences of 200 bp length were extracted using annotation from Ensembl 56. Two-hundred bp was chosen as distance, as this has been demonstrated to be optimal for the detection of enrichment, allowing for the identification of most promoter sequences without giving rise to large amounts of genetic noise (32). The comparison is performed using a hypergeometric test for the overlap of the eQTL genes with predicted FoxK2 targets. Eight-hundred fourteen out of a total of 21,459 genes have a V\$Fox\_Q2 motif with *p* < 0.05. The D8rat56 locus has a total of 48 eQTL transcripts with *p* < 0.01; 4 of them have a V\$Fox\_Q2 TF binding site (TFBS). In a hypergeometric test this leads to *p* = 0.034. The V\$Fox\_Q2 does not refer to the gene symbol but the name of the TRANSFAC matrix. The Q2 suffix is used to distinguish different versions of the same matrix, which is general for the Fox family of TFs and, therefore, also the FOXK2 ortholog in the D8Rat56 locus.

#### *Astrocyte and microglia cultures*

Primary rat astrocytes and microglia were isolated from adult brains of 10-wk-old DA and PVG rats perfused via the ascending aorta with ice-cold PBS containing heparin (LEO Pharma, Malmö, Sweden) (10 IU/ml). After removing the meninges and the cerebellum, half a brain was used and homogenized in enzymatic solution (116 mM NaCl, 5.4 mM KCl, 26 mM NaHCO<sub>3</sub>, 1 mM NaH<sub>2</sub>PO<sub>4</sub>, 1.5 mM CaCl<sub>2</sub>, 1 mM MgSO<sub>4</sub>, 0.5 mM EDTA, 25 mM glucose, 1 mM cysteine, and 20 U/ml papain, all from Sigma-Aldrich) using a microscissor. The homogenate was incubated for 60 min with gentle stirring at 37°C, 5% CO<sub>2</sub>. Next, the digested brain was transferred to a 50-ml conical tube with stopping of the enzymatic reaction by adding HBSS (Invitrogen, Stockholm, Sweden) with 10% FCS. Next, the homogenate was spun down at 200  $\times$  *g* for 7 min. The pellet was resuspended in 2 ml 0.5 mg/ml DNaseI (Roche, Bromma, Sweden) in HBSS, then filtered through a 40- $\mu$ m strainer (Becton Dickinson, Stockholm, Sweden) and transferred to 20 ml 20% stock isotonic Percoll (Sigma-Aldrich) in HBSS. Another 20 ml pure HBSS was carefully added on top to create a Percoll gradient, and the samples were then gently centrifuged at 1000  $\times$  *g* for 30 min. Thirty milliliters of the cell-containing solution beneath the top layer containing the myelin debris was collected and spun down. The resulting pellet was washed once in HBSS and the cells were resuspended in DMEM/F12 complete medium supplemented with 10% heat-inactivated FCS, penicillin-streptomycin (100 U/ml, 100  $\mu$ g/ml), 2 mM L-glutamine (all reagents from Life Technologies, Paisley, U.K.), and 20% M-CSF-conditioned L929 cell line supernatant and plated in 75-cc tissue flasks (Sarstedt, Nümbrecht, Germany) coated with poly-L-lysine (Sigma) and incubated at 37°C and 5% CO<sub>2</sub> in a humidified incubator. Medium was changed twice weekly until the cells became confluent (~14 d). When full confluence of the cell layer was reached, the mixed glial cells were harvested using prewarmed trypsin (Life Technologies, Grand Island, NY).

To separate microglia and astrocytes from each other in the mixed glial cell culture, magnetic separation was used according to the manufacturer's

instructions. In brief, the mixed cell suspension was centrifuged at  $300 \times g$  for 10 min. The cell pellet was resuspended in MACS buffer (Miltenyi Biotec, Bergisch Gladbach, Germany) and stained with PE-conjugated mouse anti-rat CD11b (BD Biosciences, Uppsala, Sweden) for 10 min. Then, the cells were washed and resuspended in MACS buffer followed by with autoMACS magnetic separation using anti-PE MicroBeads (Miltenyi Biotec). The resulting microglia (CD11<sup>+</sup> cells) and rest of the cells (astrocytes) were seeded in 24-well plates ( $4 \times 10^5$  cells/well and  $2 \times 10^5$  cells/well, respectively).

The cells (microglia and astrocytes) were then left unstimulated (only DMEM/F12 complete medium, supplemented with 10% heat-inactivated FCS, penicillin-treptomycin 100 U/ml, 100  $\mu$ g/ml), or stimulated with recombinant rat TNF- $\alpha$  (R&D Systems, Minneapolis, MN) at a concentration of 20 ng/ml (in the same medium) for 24 h, after which the cells were lysed for RNA extraction and subsequent RT-PCR expressional analysis. Astrocyte purity was checked with flow cytometry performed using a Gallios flow cytometer (Beckman Coulter, Brea, CA) with Gallios software and analyzed using Kaluza v.1.0 (both Beckman Coulter) using an FITC-labeled mouse anti-rat glial fibrillary acidic protein Ab (BD Pharmingen, Franklin Lakes, NJ). The purity was >92% in all separate experiments (data not shown). The purity of the astrocyte and microglia cultures was further assessed with RT-PCR, demonstrating very low levels of glial fibrillary acidic protein expression in the microglia cultures and barely detectable levels of Mrf-1 in the astrocyte cultures (Supplemental Fig. 1).

The TNF- $\alpha$  stimulations were also repeated on a mixed glia population to avoid one series of manipulation of the cells by separating astrocytes from microglia, and also to provide a more physiological environment and to exclude significant interference between the two cell types. In this case the cells were plated as a mixed population before the separation step, and then either left unstimulated (medium with 10% FCS only) or with TNF- $\alpha$  (20 ng/ml). The proportions of astrocytes and microglia in the mixed glia culture were 84 and 16%, respectively (Supplemental Fig. 1).

For the primary mouse astrocyte cultures, whole brains from five 10-wk-old C57BL/6 male mice were taken after PBS perfusion and removal of the meninges and the cerebellum. The protocol was identical to the rat protocol, except that the mixed glial cell population from each brain was cultured in separate culture flasks to ensure that no contamination would arise before pooling the cells. Separation of astrocytes from microglia was then performed using MicroBeads attached to an anti-mouse CD11b Ab (Miltenyi Biotec), and the astrocytes were kept, pooled, and seeded onto 24-well plates ( $2 \times 10^5$  cells/well). The astrocytes were then left unstimulated (medium only) or they were stimulated with recombinant mouse TNF- $\alpha$  (R&D Systems) at a concentration of 20 ng/ml or with TNF- $\alpha$  (20 ng/ml) together with 1 M/0.1 M/0.01 M or 0.001 M ACh chloride (Sigma-Aldrich), respectively, in medium for 24 h, after which the cells were lysed for RNA extraction and subsequent RT-PCR expression analysis. For the mouse cultures the same medium, with 10% FCS, was used as for the rats during the culture phase, but when the cells were seeded and stimulated the pH of the medium was lowered to 7.1 to increase the stability of ACh.

The concentrations used of ACh were high, because ACh is rapidly degraded by the cholinesterases acetylcholinesterase (AChE) and BChE, of which especially BChE is abundant in FCS (33). Therefore, to evaluate ACh at lower concentrations new astrocytes from adult DA rats (10 wk of age) were extracted as above and the experiments were repeated using the same medium and concentration of TNF- $\alpha$  (20ng/ml), in combination with 10 mM/10  $\mu$ M or 1  $\mu$ M ACh and 0.6 mM of the cholinesterase inhibitor eserine hemisulfate (E8625, Sigma-Aldrich; dose adopted from Ref. 34 and from personal experience [T.D.-S.]), to completely quench the activities of BChE and AChE. This increases stability of ACh, thereby allowing the usage of lower ACh concentrations. We also attempted to grow the cells without FCS, but with markedly reduced viability. Therefore, cells were initially grown with FCS, but with the stimulation steps performed without FCS. However, also here cell viability was too low to allow for reliable results.

#### Analysis of C3 protein levels

Primary astrocyte and microglia cultures were established from three DA rats as described above. A pilot experiment indicated that C3 levels would be low, and therefore a 48-h stimulation protocol was used. After plating, the cells were left unstimulated (medium only) or they were stimulated with 20 ng/ml TNF- $\alpha$  or TNF- $\alpha$  together with 1 M/0.1 M/0.01 M or 0.001M ACh chloride in medium using 500  $\mu$ l/well instead of 1 ml. After 24 h an additional 500  $\mu$ l of the same type of medium was added to the respective well, and after another 24 h the cells were processed for RT-PCR and the supernatants collected for protein quantification. Quantification of C3 protein levels in the undiluted cell supernatants was performed using a rat C3 ELISA kit (GenWay Biotech, San Diego, CA) according to the manufacturer's instructions. The lowest concentration of the standard was 12.5 ng/ml and was in the linear range of detection. All samples were

analyzed in duplicate, with a maximum variability between duplicates of <10% even at the lowest concentrations. Additionally, the experiment was repeated to confirm the reliability of the results, with a similar outcome.

#### Statistical analysis

The software program R 2.6.0 was used for statistical analyses and graphs depicting eQTL localization using the package qtl1.14-2. For all other analyses significance levels were calculated using an unpaired *t* test, except for the *in vitro* data, where one-way ANOVA was used, with Bonferroni post hoc comparisons, all performed using the GraphPad Prism 5.0 (GraphPad Software, San Diego, CA). In general,  $p < 0.05$  was considered statistically significant, except for in the microarray analysis, where  $p < 0.01$  was used with permutation analyses (described above).

## Results

### Characterization of complement kinetics, localization, and effects following CNS injury

We have previously demonstrated substantial differences in neuronal survival and complement expression in the spinal cords from the inbred rat strains DA and PVG following VRA (14, 24, 35). A more detailed characterization of the expression of the key complement components C1q and C3 was here performed in DA and PVG rats following VRA, which demonstrated both a genetic and temporal component governing expression. Peak expression of C1q occurred at 3 d and C3 at 7 d after injury, whereas C1q expression was higher in the DA strain only at 5 d, and C3 expression was higher in the DA strain at most studied time points (Fig. 1A, 1B). *In situ* hybridization for C3 at 5 d after VRA displayed a diffuse signal pattern in the ventral horn, which did not permit localization of expression to discrete cell populations, but was indicative of glial expression, but not motor neurons (Fig. 1C–I).

Downstream activation of the complement cascade leads to chemotactic signals for immune cells and formation of the MAC (1, 3, 4). As a positive control for activation of the entire complement cascade, we examined the response in a controlled-contusion TBI model, which is well established to induce complement activation (8, 36, 37). Presence of neutrophils, as shown by MPO immunolabeling, was evident after TBI but not VRA (Fig. 2C–F). Similarly, MAC immunopositive neurons were present in the vicinity of the TBI lesion, but not in the ventral horn after VRA (Fig. 2G, 2H).

Lastly, expression of CD59, a potent complement inhibitor, was examined after VRA, showing stable or downregulated levels after injury, without clear strain differences (Supplemental Fig. 2A). *In situ* hybridization of CD59, as opposed to C3, clearly localized CD59 expression to motor neurons (Supplemental Fig. 2C–F).

Thus, increased expression of upstream complement components in VRA did not occur in the context of MAC activation or neutrophil infiltration. However, because both C1q and C3 are implicated in the removal of synapses (38), we assessed synaptic density 5 d after VRA. Synaptophysin-immunoreactive cell elements were quantified in the ventral horn demonstrating decreased labeling intensity in DA rats compared with PVG rats, suggesting a greater and more rapid loss of synapses (Fig. 3A–F). Furthermore, increased C3 immunoreactivity in the lesioned ventral horn was evident in very close proximity to axotomized motor neurons (Fig. 3G–I). This suggests that increased local complement expression following VRA is associated with increased synapse elimination, but not neutrophil infiltration or MAC activation.

### Dissection of genetic pathways regulating complement expression

The finding of genetically governed differences in local complement expression motivated an effort to identify underlying genes

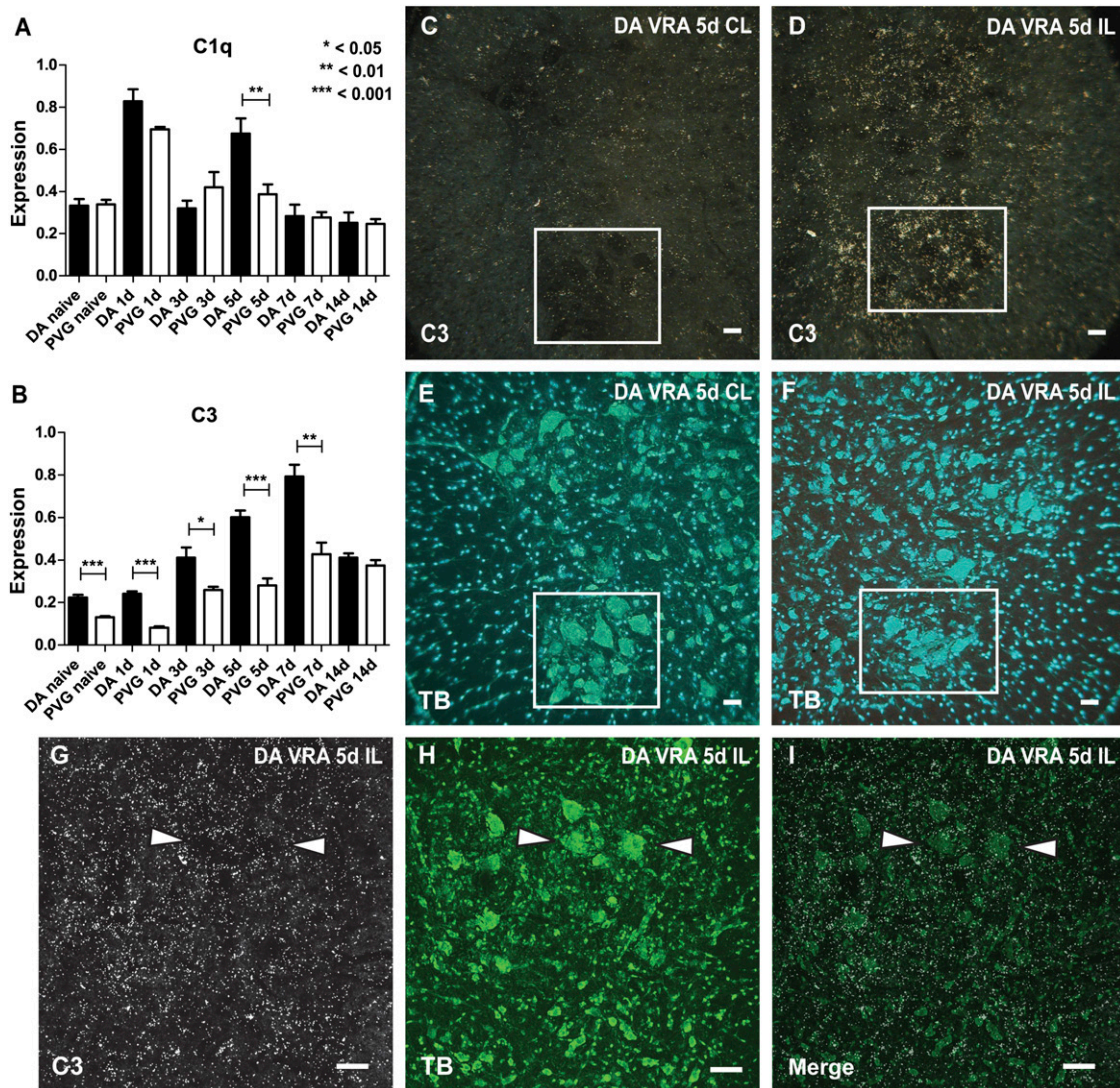


**FIGURE 1.** Regulation of C1q and C3 in DA and PVG rats after ventral root avulsion. Local expression levels of C1q (A) and C3 (B) were determined with RT-PCR in the injured spinal cord of DA and PVG rats at different time points following ventral root avulsion and demonstrate strain-dependent regulation with higher levels in the DA strain. Complement expression is upregulated in both strains following injury, with peak expression of C3 occurring later than for C1q. (C–I) In situ hybridization for C3 mRNA in the ventral horn of the ipsilateral (IL) side shows higher labeling density in the IL compared with the contralateral side (C–F); the white box delineates the ventrolateral motor neuron pool. The hybridization signal is present over glial cells rather than motor neurons (C–I); the white arrows point at selected motor neurons. TB; toluidine blue, background staining. Scale bars, 40  $\mu$ m.

and/or pathways. This can be done by QTL mapping in an  $F_2$  intercross, created by systematically crossing the strains (15, 39). Additionally, the combination of trait linkage analysis with mapping of eQTL using powerful global expression profiling techniques has proven useful for gene positioning (40).

Consequently, an  $F_2$ (DA  $\times$  PVG) intercross was bred, and global expression profiling of spinal cords from 144  $F_2$  animals 5 d after VRA was performed. Five days was chosen, as the kinetic studies identified this as a time point with intense complement activation. The  $F_2$  intercross was genotyped throughout the genome with microsatellite markers revealing a total of 3418 eQTL at a  $p < 0.01$  for genome-wide significance level, with 776 regulated in *cis* and the remaining in *trans*.

Most complement components, such as C1r and C1s as well as C2, C5, C7, C8b, C8g, and the complement regulatory proteins CD59, CD46, CD55, factor H, and clusterin, did not display linkage with  $p < 0.01$  to any of the genomic markers.

In contrast, the expression of C1qa, C1qb, C3, and C9 all displayed regulation from distinct gene regions. The genes encoding

C1qa and C1qb are localized next to each other, adjacent to the *C1qc* gene, on rat chromosome 5 at  $\sim 155.6$  Mb. Expression of C1qa, along with a cluster of 47 other genes, was regulated in *trans* from D4Got130 ( $p < 0.01$ ) (Fig. 4A, 4B) on rat chromosome 4 (166.1 Mb). Several of the other transcripts regulated from this marker are also related to innate immune function, such as CLEC domain family 4 member A isoform 3 (Clec4a3, also known as Dcir3), Clec4a2 (also known as Dcir2), and three different killer cell lectin-like receptors (KLRs; Klra2, Klrc1 and Klrk1), all of which were regulated in *cis* (Table II). Expression of C1qa was higher in animals with DA alleles at D4Got130, whereas the CLEC transcripts were higher in animals carrying PVG alleles. The D4Got130-regulated gene cluster was highly significantly enriched for carbohydrate binding and wound healing ( $p < 0.001$ ).

C1qb was regulated in *trans* from the marker D4Rat25 ( $p < 0.01$ ) (Fig. 4C, 4D) located at 65.8 Mb on chromosome 4, together with 33 other genes (Table III), including Clec2l and Clec5a, both regulated in *cis* (both  $p < 0.001$ ). This cluster, comprising 34 genes, was enriched for sugar binding ( $p < 0.01$ ). Expression of C1qb and

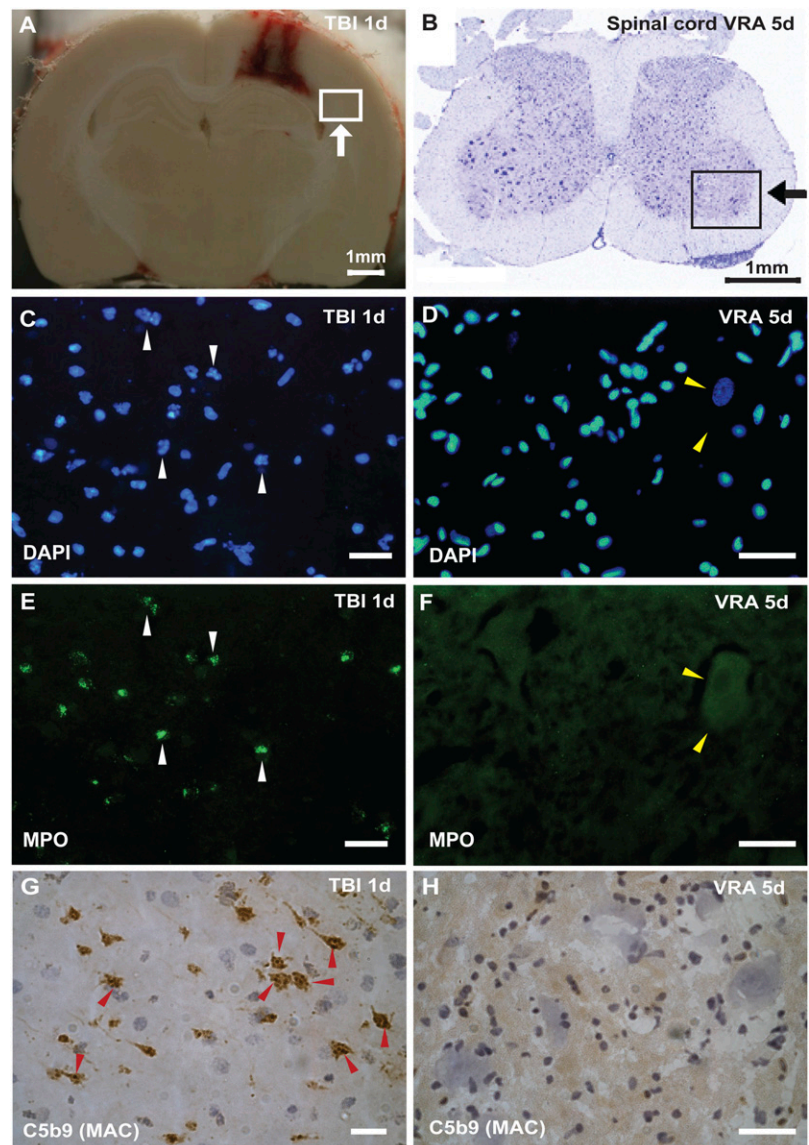


**FIGURE 2.** Evidence of MAC activation and neutrophil infiltration following TBI but not VRA. Coronal section of the DA rat brain 1 d after TBI (**A**); boxed area shown in higher magnification in (**C**), (**E**), and (**G**). DA spinal cord 5 d after VRA (**B**); boxed area shown in higher magnification in (**D**), (**F**), and (**H**). Cell nuclei staining of the injured brain (**C**; the white arrowheads show the segmented nuclei of infiltrating neutrophils) and spinal cord (**D**; the yellow arrowheads show the large nucleus of a motor neuron). Immunoreactivity for MPO confirms extensive infiltration of neutrophils in the injured brain (**E**), whereas no neutrophils are found in the spinal cord following VRA (**F**). In the injured brain, C5b-9 (MAC) immunoreactivity is present on neurons, marked with red arrowheads (**G**) but not in the spinal cord after VRA (**H**). Scale bars, 40  $\mu\text{m}$  unless specified otherwise.

Clec2l were higher in animals with DA alleles in D4Rat25, whereas expression of Clec5a was higher in animals with PVG alleles.

C9, the only downstream complement component with significant genomic linkage, was regulated from the marker D3Rat44 on chromosome 3 (41.4 Mb) (Fig. 5A, 5B). The cluster comprises 129 genes (Table IV) and is enriched for multiple biological processes. All genes in this cluster were regulated in *trans*, except for CD302 (also called Clec13A or Dcl-1) and  $\alpha_6$  integrin (also called VCAM-6, transcript ID 10836849). Expression of C9 was higher in animals carrying DA alleles at D3Rat44, whereas expression of CD302 was higher in animals carrying PVG alleles.

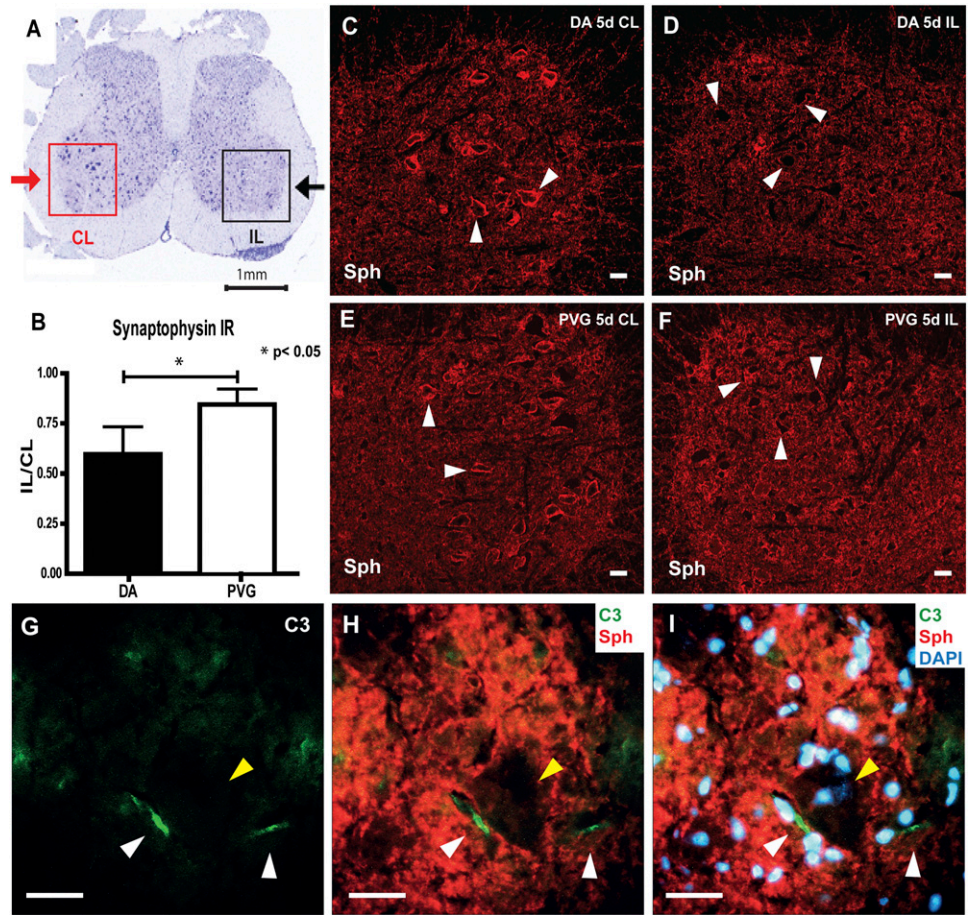
The pattern of linkage to *cis*-regulated CLEC gene regions was different for the key complement protein C3. Thus, C3, itself located on chromosome 9, was regulated in *trans* from the marker D8Rat56 ( $p < 0.01$ ) (Fig. 5C, 5D), at the beginning of chromosome 8 (8.2 Mb), with higher expression in animals carrying DA alleles at D8Rat56. Expression of C3 was co-regulated with 47 other genes, none of which belongs to the CLEC family, and many were unannotated (Table V). This cluster differed in that it did not show any specific enrichment. However, most transcripts in the cluster were interconnected, as identified by studying pairwise correlation of expression. The constructed *trans* eQTL gene expression network provides information about the dependency

structure between transcripts (Fig. 6), and strongly connected hub genes can be identified and constitute candidates for being master regulators (41). Only five of the genes in the network were physically located in the genetic region of D8Rat56. One of these five genes, F1M641\_RAT, is functionally annotated as a TF (transcript ID 10908220; Ensembl gene ID ENSRN0G00000039894) orthologous to human FOXX2, and it therefore constitutes a candidate for regulating the *trans*-cluster. This was assessed by analyzing TFBS predictions, following the hypothesis that genetic changes of gene expression of TFs will affect the expression of their direct targets (29). A significant enrichment of TFBS for the FOXX2 ortholog was found in the 200-bp putative promoters of four of the *trans*-regulated transcripts ( $p = 0.034$ ) in the D8Rat56 cluster (see also Materials and Methods): BChE, Spdya, and two unannotated transcripts, 10718155 and 10937323. The C3 gene was not predicted as a direct target of the FOXX2 ortholog, but it was connected by way of its co-regulation with BChE expression (Fig. 6).

#### *Expression of a FOXX2 ortholog and BChE after a standardized nerve injury*

Expression of the FOXX2 ortholog as shown by RT-PCR demonstrates an initial upregulation at 1 d after injury, with a subsequent drop to levels below those of naive controls and with higher

**FIGURE 3.** Complement activation is associated with loss of synaptic immunostaining. Micrograph of a spinal cord section after ventral root avulsion, with the ipsilateral (IL) side marked with a black box and the contralateral (CL) side marked with a red box (A). The synaptophysin immunoreactivity signal ratio of IL/CL sides, reflecting loss of synaptic terminals, is reduced to a greater extent in DA compared with PVG at 5 d after VRA (B). Micrographs showing synaptophysin immunolabeling in the ventral horn of the lesioned and unlesioned sides in DA and PVG rats demonstrate a marked loss of the signal outlining the contour of lesioned motor neurons in both strains (C–F; arrowheads indicate motor neurons). Immunolabeling for C3 (G) and synaptophysin (H) demonstrates C3 deposition (white arrowheads in (G)–(I)) on the contour of an axotomized motor neuron (yellow arrowheads in (G)–(I)). The merged image with DAPI staining shows clusters of glial cells around the axotomized motor neuron (I). Scale bars, 40  $\mu$ m.



expression in PVG rats at 3, 7, and 14 d after injury (Fig. 7A). As for C3, BChE was more highly expressed in the DA strain at most studied time points, and it peaked at 7 d after injury (Fig. 7B),

when expression of the FOXC2 ortholog was at its lowest. BChE immunoreactivity was evident in the cytoplasm of axotomized motor neurons (Fig. 7D, 7F). Additionally, BChE colocalized with

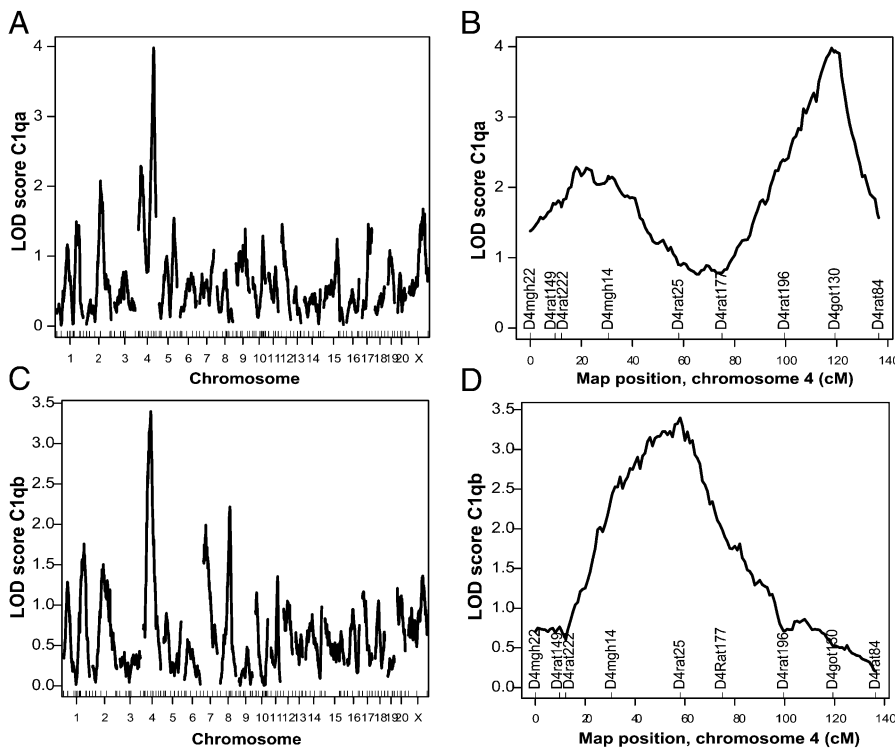


**FIGURE 4.** Expression of complement components C1qa and C1qb is regulated from distinct gene regions. The expression of C1qa is *trans*-regulated from chromosome 4 (A), with D4got130 as peak marker (B). Expression of C1qb is also *trans*-regulated from chromosome 4 (C), but from another region with D4rat25 as peak marker (D). The x-axis marks the chromosome numbers in (A) and (C) and the genetic distance in centiMorgans in (B) and (D). The y-axis marks the significance of the linkage, here shown in logarithm of odds (LOD) scores, where an LOD of >3.1 is considered significant.

Table II. List of genes regulated from marker D4Got130

Gene/Transcript ID	eQTL Marker	<i>p</i> Value	Gene/Transcript ID	eQTL Marker	<i>p</i> Value
10701663	D4Got130	0.0085	Hist1h4m_predicted	D4Got130	0
10756873	D4Got130	0.001667	Hist1h4m_predicted	D4Got130	0
10781960	D4Got130	0.009336	<b>Klra2</b>	D4Got130	0
10830544	D4Got130	0.009	<b>Klrcl1</b>	D4Got130	0
10859203	D4Got130	0	<b>Klrk1</b>	D4Got130	0
10859382	D4Got130	0.000127	LOC679752	D4Got130	$5.00 \times 10^{-4}$
10859627	D4Got130	0.000353	LOC683001	D4Got130	0.000423
10892141	D4Got130	0.008	Loh12cr1	D4Got130	$2.00 \times 10^{-6}$
Aacs	D4Got130	0.002	Nefh	D4Got130	0.005
Arhgdib	D4Got130	0	Ninj2	D4Got130	$2.00 \times 10^{-5}$
Bace1	D4Got130	0.000786	Ntng1	D4Got130	0.000417
Bcat1	D4Got130	0.007333	Pgap1	D4Got130	0.008
Bspry	D4Got130	0.0075	Pik3ca	D4Got130	0.004
<b><i>C1qa</i></b>	D4Got130	0.003667	Ptpdc1	D4Got130	0.003
Ccdc77	D4Got130	0	Rbks	D4Got130	0.0085
<b>Clec4a3</b>	D4Got130	0	Rcc2_predicted	D4Got130	0.002167
Cltn3	D4Got130	$1.00 \times 10^{-6}$	RGD1559643	D4Got130	0.007
Cx3cl1	D4Got130	0.0096	Rps4y2	D4Got130	0.000428
<b>Dcir2</b>	D4Got130	0.004667	Rtkn	D4Got130	0.006
Eno2	D4Got130	0.001571	Scgb3a1	D4Got130	0.0065
Fam80b	D4Got130	0.006667	Slc4a5	D4Got130	0.000606
Gabarapl1	D4Got130	0	Sln	D4Got130	0.000909
Gnb4	D4Got130	0.001571	Vamp3	D4Got130	0.001111
Grlh3	D4Got130	0.007	Znf397_predicted	D4Got130	0.001111

The CLEC genes (Clec4a3/Dcir3 and Clec4a2/Dcir2) and the KLR genes (Klra2, Klrcl1, and Klrk1) are marked in bold type. C1qa is in bold type, italic, and underlined.

vWF in small blood vessels (Fig. 7E). Apart from being *trans*-regulated from D8Rat56, BChE expression was also *cis*-regulated from D2Rat44 ( $p = 5.1 \times 10^{-5}$ ), with higher expression in DA allele homozygous rats.

The FOXK2 ortholog has a paralog in rat, FoxK2 (ENSR-NOG0000036663), which is a larger gene (4632 bp, 580 aa) compared with the ortholog (741 bp, 246 aa). However, the DNA-binding FOX domains spanning bp 247–344 in the FoxK2 gene and bp 202–246 in the FOXK2 ortholog show a 96% sequence homology both at the nucleotide and amino acid levels (<http://blast.ncbi.nlm.nih.gov>, [www.ensembl.org](http://www.ensembl.org), and University of California Santa Cruz genome browser; <http://genome.ucsc.edu>), suggesting that they could interact with similar TFBS. Expression of both rat FoxK2 and the ortholog was downregulated after injury in the parental strains; however, only the ortholog displayed an initial up-regulation and subsequent strain difference, with higher expression

in PVG animals, at later time points (Fig. 7A, 7C). There are no available Abs for the ortholog; however, staining with a rat FoxK2 Ab shows labeling of motor neurons (Fig. 7G, 7H).

#### *The expression of C1q and C3 is differentially regulated in cultured glia*

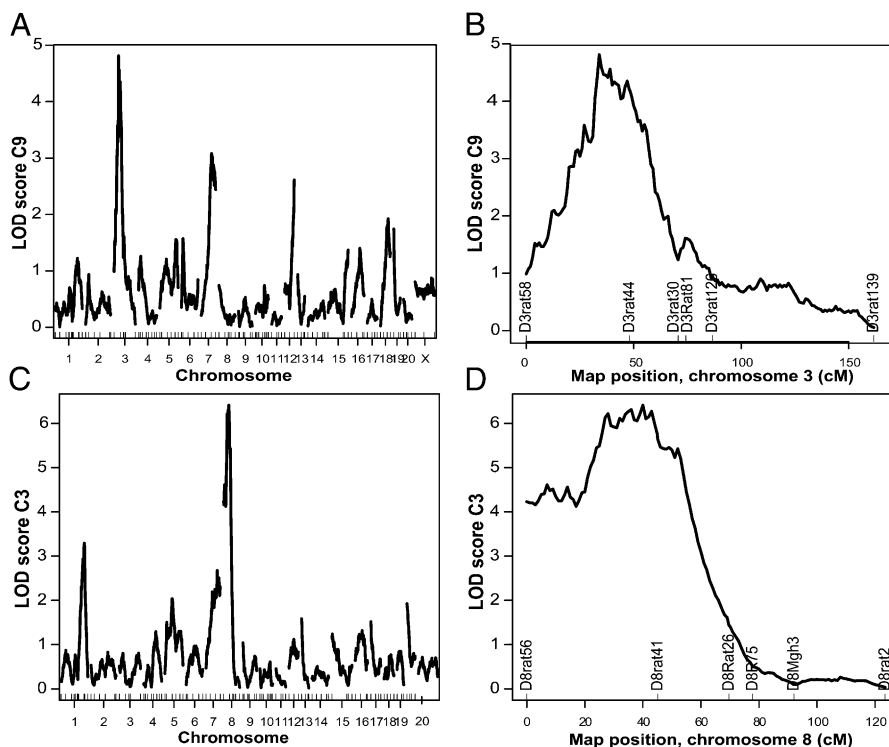
The C3 in situ hybridization patterns suggested a glial origin of expression. Therefore, astrocyte and microglia cell cultures from rats and astrocyte cultures from mice were established to functionally explore regulation of C3, as well as of C1q, in vitro. Because ACh is known to regulate inflammatory responses through TNF- $\alpha$  pathways (42, 43) and is hydrolyzed by BChE, we hypothesized that C3 might be regulated by TNF- $\alpha$  and ACh. Astrocyte and microglia cells from adult DA and PVG brains were stimulated with TNF- $\alpha$ , which resulted in a strong increase in C3 expression in both astrocytes and microglia (Fig. 8A, 8B).

Table III. List of genes regulated from marker D4Rat25

Gene/Transcript ID	eQTL Marker	<i>p</i> Value	Gene/Transcript ID	eQTL Marker	<i>p</i> Value
Abcg2	D4rat25	0	Mocos	D4rat25	0.006533
Atp6v0e2	D4rat25	$3.7 \times 10^{-5}$	Ptgds2	D4rat25	$4.4 \times 10^{-5}$
Bcl2l14	D4rat25	0.003333	RGD1310827	D4rat25	0.001714
<b><i>C1qb</i></b>	D4rat25	0.0065	RGD1311849_predicted	D4rat25	0.003667
<b>Clec2l</b>	D4rat25	0.000182	RGD1564149	D4rat25	0.009
<b>Clec5a</b>	D4rat25	0.000478	RGD1566215_predicted	D4rat25	0.000333
Dennd2a	D4rat25	0.005	Sema6b	D4rat25	0.007
Diol1	D4rat25	0.00125	Slc4a5	D4rat25	0
Dpt	D4rat25	0.000769	Snx10	D4rat25	0
Dzip1	D4rat25	0.0075	Taldo1	D4rat25	0.000361
Gimap9	D4rat25	0.00275	Tmem176a	D4rat25	0.0025
Grip2	D4rat25	$6.4 \times 10^{-5}$	Tmem176b	D4rat25	0
Grn	D4rat25	0.0055	Tnp1	D4rat25	0.0055
Kcna10_predicted	D4rat25	0.0025	Tomm20	D4rat25	0.003667
Kifc1	D4rat25	0.0035	Uqcrfs1	D4rat25	0.005333
LOC500077	D4rat25	0.000262	Wbscr17	D4rat25	0.007
LOC685322	D4rat25	0.00037	Zswim5	D4rat25	0.0065

C1qb is in bold type, underlined, and italic; the CLEC genes (Clec2l and Clec5a) are in bold type.

**FIGURE 5.** Expression of complement components C9 and C3 is regulated from distinct gene regions. The expression of C9 is *trans*-regulated from chromosome 3 (A), with D3Rat44 as peak marker (B). The expression of C3 is *trans*-regulated from chromosome 8 (C), with D8Rat56 as peak marker (D). The x-axis marks the chromosome numbers in (A) and (C) and the genetic distance in centiMorgans in (B) and (D). The y-axis marks the significance of the linkage here shown in logarithm of odds (LOD) scores, where an LOD of >3.1 is considered significant.



In contrast, the expression of C1q was not affected by TNF- $\alpha$  (Fig. 8C, 8D), corroborating the findings from the eQTL mapping demonstrating different regulatory mechanisms for C1q and C3. Notably, only astrocytes displayed strain differences in the expression of C3. TNF- $\alpha$  also increased the expression of C3, but not C1q, in mouse astrocytes (Fig. 8E, 8F). Furthermore, ACh-attenuated TNF- $\alpha$  induced C3 expression in a dose-dependent manner, which provides additional support for the role of cholinergic/TNF- $\alpha$  pathways in the regulation of C3 (Fig. 8G).

Finally, to confirm the effect of ACh in suppressing C3 upregulation following inflammatory stimulation also at the protein level, we analyzed C3 levels in the culture supernatants and expression in cells after 48 h of stimulation of primary astrocyte and microglia cultures (Fig. 9A, 9B). The levels of C3 protein correlated with the C3 mRNA expression levels (Fig. 9C, 9D) in both astrocytes and microglia. Furthermore, in both astrocyte and microglia cultures there was a clear dose-response effect with abrogation of the TNF- $\alpha$  effect on C3 levels with increasing concentration of ACh. In astrocyte cultures the C3 protein levels were detectable only in cultures stimulated with TNF- $\alpha$  alone or in combination with the lowest tested ACh concentration (Fig. 9A).

The concentrations used for these experiments were high owing to the presence of cholinesterases (ChE) in the culturing medium, released by the cells themselves or from the added FCS. Therefore, the experiments were repeated; first with astrocytes stimulated with TNF- $\alpha$  and lower concentrations of ACh in the presence of a cholinesterase inhibitor (eserine hemisulfate), which confirmed that ACh inhibits C3 expression after TNF- $\alpha$  stimulation also at lower concentrations (Fig. 10A). Next, a mixed glial culture was stimulated with TNF- $\alpha$  to verify that C3 upregulation occurred also in a mixed cell culture more similar to the *in vivo* situation (Fig. 10B).

## Discussion

To dissect the variability in expression of complement components in the CNS occurring naturally between two inbred rat strains, we

performed an extensive eQTL mapping in a large F<sub>2</sub> intercross. This revealed distinct gene regions regulating expression of several complement components as well as a hitherto unknown connection between C3 and the cholinergic system.

The most acknowledged effector function of the complement system is the downstream assembly of the MAC (3, 4), which has been demonstrated after traumatic brain and spinal cord injuries (8, 44). In the present study we could not detect signs of MAC activation or recruitment of neutrophils after VRA. In contrast, both of these were present after experimental TBI, likely due to the more drastic loss of blood–brain barrier function. Nevertheless, intrinsic CNS complement expression may contribute to neurodegenerative processes occurring after injury, as local activation of the complement components C1q and C3 has been shown to be involved in the removal of nerve terminals during development and in certain neurodegenerative models of the adult animal (38). In the context of nerve avulsion, we have previously found a positive correlation between the local expression of C1q and loss of motor neurons (14). In the present study we found an association with a preceding neurodegenerative phenomenon in the form of elimination of synaptic terminals at the time point when expression of C1q and C3 peaks. The upregulation of complement occurs locally, in the injured CNS, although it cannot be excluded that infiltrating cells, in particular monocytes/macrophages, may contribute. Taken together, these results support the notion that genetic heterogeneity in the regulation of the complement system may contribute to synapse elimination and removal of degenerating cells after nerve injury.

The combination of large-scale breeding and global expression profiling used in the present study identified a novel TF from the FOX family regulating a network of transcripts including C3. Because the C3 promoter lacks a FOXK2 binding site, C3 regulation is likely to be a downstream event. Interestingly, the network analysis puts C3 downstream of BChE, a choline esterase with multiple functions in the CNS, not the least of which is degradation of ACh (45). Expression of the FOXK2 ortholog was

Table IV. List of genes regulated from marker D3Rat44

Gene/Transcript ID	eQTL Marker	p Value	Gene/Transcript ID	eQTL Marker	p Value
10709744	D3rat44	0.002	Lpcat4	D3rat44	0.003018
10714420	D3rat44	0.005	Lrrc55	D3rat44	0.001776
10716537	D3rat44	0.00275	Lrsam1	D3rat44	0.0025
10729122	D3rat44	0.002	Mab2111	D3rat44	0.003667
10741356	D3rat44	0.004333	Mageb16	D3rat44	0.004333
10749861	D3rat44	0.000345	Nob1	D3rat44	0.004333
10754140	D3rat44	0.007	Nup210l	D3rat44	0.001375
10756328	D3rat44	0.0065	Olr1118	D3rat44	0.005
10763732	D3rat44	0.00125	Olr1251	D3rat44	0.00325
10775780	D3rat44	0.0065	Olr1286	D3rat44	0.0065
10780144	D3rat44	0.000833	Olr1341	D3rat44	0.00275
10790710	D3rat44	0.005	Olr1358	D3rat44	0.003333
10791573	D3rat44	0.007	Olr1539	D3rat44	0.003667
10798220	D3rat44	0.005667	Olr160	D3rat44	0.001667
10802587	D3rat44	0.007	Olr1679	D3rat44	0.000156
10825571	D3rat44	0.0085	Olr1687	D3rat44	0.006
<b>10836849, Itga6</b>	D3rat44	0.000556	Olr181	D3rat44	0.004667
10862932	D3rat44	0.001667	Olr341	D3rat44	0.003
10869391	D3rat44	0.0085	Olr383	D3rat44	0.003667
10877538	D3rat44	0.0025	Olr395	D3rat44	0.00325
10877687	D3rat44	0.0075	Olr502	D3rat44	0.0095
10887400	D3rat44	0.001714	Olr551	D3rat44	0.0065
10893395	D3rat44	0.009	Olr581	D3rat44	0.00325
10893399	D3rat44	0.003	Olr672	D3rat44	0.004333
10897604	D3rat44	0.0025	Olr716	D3rat44	0.001375
10917984	D3rat44	0.004	Olr729	D3rat44	0.002667
10926847	D3rat44	0.005	Olr783	D3rat44	0.005333
10932719	D3rat44	0.006	Olr82	D3rat44	0.001444
10934310	D3rat44	0.004667	Olr84	D3rat44	0.006
10939734	D3rat44	0.0055	Olr848	D3rat44	0.007
10939799	D3rat44	0.0075	Olr89	D3rat44	0.0022
Aox4	D3rat44	0.003429	Pdia3	D3rat44	0.003552
Aurkb	D3rat44	0.00975	Pkd2l2	D3rat44	0.008
B4galnt3	D3rat44	0.004	Prss34	D3rat44	0.003333
Bat5	D3rat44	0.005	Ptpn3	D3rat44	0.0028
Bcl9	D3rat44	0.006	Rbm18	D3rat44	0.000569
Brf1	D3rat44	0.0028	RGD1305184_predicted	D3rat44	0.0034
<b><u>C9</u></b>	D3rat44	0.000263	RGD1309759_predicted	D3rat44	0.0065
Ccndbp1	D3rat44	0.002231	RGD1310257_predicted	D3rat44	0.0065
<b>Cd302, Clec13a</b>	D3rat44	0	RGD1560330_predicted	D3rat44	0.000667
Ciapiin1	D3rat44	0.0055	RGD1562088_predicted	D3rat44	0.000556
Commmd4	D3rat44	0.002	RGD1562433	D3rat44	0.006
Crygb	D3rat44	0.0026	RGD1564827_predicted	D3rat44	0.005333
Defa9	D3rat44	0.004333	RGD1565927_predicted	D3rat44	0.0055
Defcr24	D3rat44	0.000476	Scara3	D3rat44	0.001833
Doxl1	D3rat44	0.004	Sh2d4a	D3rat44	0.004333
Fear	D3rat44	0.003333	Sqrdl	D3rat44	0.001281
Gatad2b	D3rat44	0.0055	Tas2r40	D3rat44	0.0085
Glb1l	D3rat44	0.0085	Tat	D3rat44	0.0075
Got1	D3rat44	0.0055	Tbx22	D3rat44	0.0055
Il2ra	D3rat44	0.0065	Tceb1	D3rat44	0.003333
Irak3	D3rat44	0.001375	Tgfb3	D3rat44	0.003812
Klb_predicted	D3rat44	0.000125	Timm8a2	D3rat44	0.00275
Klkb1	D3rat44	0.005	Tpsab1	D3rat44	0.003
LOC290704	D3rat44	0.002	Trim47l	D3rat44	0.008
LOC297568	D3rat44	0.0095	Ucn3	D3rat44	0.001833
LOC302760	D3rat44	0.0025	Umod	D3rat44	0.004
LOC305698	D3rat44	0.009	V1rc43	D3rat44	0.000647
LOC363694	D3rat44	0.004667	V1re12	D3rat44	0.0095
LOC363964	D3rat44	0.000458	Wdr64	D3rat44	0.00425
LOC685109	D3rat44	0.0025	Vom2r10	D3rat44	0.008
LOC688299	D3rat44	0.006	Vom2r28	D3rat44	0.0065
LOC689081	D3rat44	0.007471	Zc3hc1	D3rat44	0.008
LOC689604	D3rat44	0.000238	Zfp819	D3rat44	0.00275
LOC689770	D3rat44	0.005			

The two *cis*-regulated genes in the cluster, Cd302/Clec13a and Itga6, are marked in bold type. C9 is bold type, italic, and underlined.

lowest at 7 d after injury, a time point when the expression of both BChE and C3 peak. Arguably, our experimental data suggest a chain of events that starts in axotomized neurons with a change in transcription factor activity affecting, among other things,

BChE transcription. Apart from its role as a neurotransmitter, ACh also exerts effects on glial activation status and attenuates neuroinflammation by modulating TNF- $\alpha$  pathways (46) through nicotinic ACh receptors (47). Interestingly, altered BChE ac-

Table V. List of genes regulated from marker D8Rat56

Gene/Transcript ID	eQTL Marker	<i>p</i> Value	Gene/Transcript ID	eQTL Marker	<i>p</i> Value
10702714	D8rat56	0	Deps	D8rat56	$1.00 \times 10^{-6}$
10702716	D8rat56	$2.4 \times 10^{-5}$	Defb15	D8rat56	0.0075
10711987	D8rat56	0.000233	Fam154b	D8rat56	0.007
<b>10718155</b>	D8rat56	0.0055	Gcdh	D8rat56	0.0065
10725567	D8rat56	0.004667	Imp3	D8rat56	$4.00 \times 10^{-6}$
Smtnl2	D8rat56	0.004203	Krt40	D8rat56	0.0055
Alpk1_predicted	D8rat56	0.003667	LOC680045	D8rat56	0.0035
10888299	D8rat56	0.0065	LOC686922	D8rat56	0.004
10894268	D8rat56	0.0022	LOC688553	D8rat56	0.004333
<b>10908220</b>	D8rat56	0.002	Mfi2	D8rat56	0.006
10914937	D8rat56	0.001833	Mrpl4	D8rat56	0.000909
10915003	D8rat56	0.0065	Mrpl44	D8rat56	0.003333
10915103	D8rat56	$3.7 \times 10^{-5}$	Olr1417	D8rat56	0.0065
10915105	D8rat56	0	Pmpcb	D8rat56	0.005
10916458	D8rat56	0.000696	Rbak	D8rat56	0.007
10918270	D8rat56	0.003667	RGD1305138	D8rat56	0.004
<b>10937323</b>	D8rat56	0.0075	RGD1311723	D8rat56	0
LOC302759	D8rat56	0.0065	RGD1563216	D8rat56	0.003
<b>Bche</b>	D8rat56	0.007153	Sh3bp4	D8rat56	0.004
Bcl2l2	D8rat56	0.004	<b>Spdya</b>	D8rat56	0.009
<b>C3</b>	D8rat56	0.001257	Srpr	D8rat56	0.003169
Calhm1	D8rat56	0.0055	Tmem128	D8rat56	0.006
Cdh20	D8rat56	0.005	Trex2	D8rat56	0.0085
Cyp2d3	D8rat56	0.003667	Vps4a	D8rat56	0.0075

The transcription factor orthologous to FOXK2 is in bold type and underlined, and the genes with binding sites for the transcription factor (10718155, 10937323, Bche, and Spdya) are in bold type. C3 is in bold type, underlined, and italic.

tivity has been associated both with Alzheimer disease (48), where loss of synapses correlates with cognitive deterioration (49) and recently also to multiple sclerosis (50). Previous data demonstrate that in the rat spinal cord BChE is mainly expressed in motor neurons (51), corroborated in the present study by the finding of BChE immunoreactivity in axotomized motor neurons. Unlike many other molecules involved in synaptic transmission, the expression of BChE was increased in the ventral horn on the lesioned side and was also higher in DA compared with PVG strains both in naive and injured animals. The localization of BChE in lesioned motor neurons and C3 in close proximity to the cell surface, where synaptophysin immunoreactivity is decreased compared with uninjured cells, provides a spatial relationship between these molecules. However, many additional genetic influences acting on this pathway are probable, because, for example, the expression of BChE is also *cis*-regulated from its location on chromosome 2.

The suggested role of BChE as a regulator of inflammatory responses is interesting, as we recently identified BChE as a potential regulator of glial activation in Alzheimer disease (52). Recent studies underscore the importance of cholinergic signaling for regulating adaptive immune responses (43), where TNF- $\alpha$  is a key mediating factor (46). TNF- $\alpha$  has also been linked to a both faster and more severe disease course in Alzheimer disease (53), as well as to modulation (54) and degradation of synapses (55). We could in this study record a strong induction of C3 expression upon stimulation with TNF- $\alpha$  in astrocyte and microglia cultures. This was not the case for C1q, supporting the notion that C1q and C3 are regulated in different ways. Also, ACh suppressed the TNF- $\alpha$  effect on C3 both at the mRNA and protein levels, suggesting a role for cholinergic pathways in regulating complement C3 expression in the CNS, although the C3 protein levels in astrocytes were just below the described detection range and should be interpreted with some caution. Presumably, the observed actions of ACh are exerted through nicotinic  $\alpha 7$  ACh receptors, known to be expressed on glial cells and to modulate

inflammatory responses (56), although formal proof is not provided in the present study. The levels of ACh used in the initial experiments were high, although concentrations of at least 0.35 mM ACh have been reported in the cytoplasm of individual cholinergic neurons in *Aplysia* (57). Extracellular levels of ACh are even more difficult to define, given the abundance, and efficiency of the cholinesterases (AChE and BChE) (58, 59), and also the physiological variations due to neuronal activity. Extracellular basal levels are in the nanomolar range, but they can increase to the micromolar range after inhibiting ChEs (59, 60). Also, in mutant mice partially deficient for AChE, basal extracellular levels of ACh were in the micromolar range without signs of toxicity (61). Blocking ChE activity led to effects on C3 expression at much lower ACh concentrations, suggesting that the high concentrations of ACh used initially were necessary to avoid complete depletion of ACh by ChEs present in the medium. Lastly, FCS was needed in the cell culture experiments, and we can therefore not rule out additional influence of the FCS on complement expression in glia, although FCS was used in all conditions, that is, also in unstimulated cells. Therefore the observed increase in complement expression following TNF- $\alpha$  stimulation is indeed likely a TNF- $\alpha$ -specific effect.

The gene expression analysis puts a new TF from the FOX gene family at the center of the network regulating C3. This group of transcription factors plays important roles in many important biological processes (62), not least in immune responses (63), where FoxP3 has been extensively studied as a marker for regulatory T cells (64). Fox genes are expressed in the CNS (65), and FOXK2, also known as ILF1, was first found to bind the IL-2 promoter (66), where it was shown to function as a repressor of IL-2 transcription in resting T cells (67). The fact that the FOXK2 ortholog was downregulated from day 3 after injury, coinciding with increased expression of BChE and C3, supports its role as a suppressor of transcription. However, further studies are needed to elucidate more in detail the role of the FOXK2 ortholog and its paralog in regulation of inflammatory responses in the CNS.

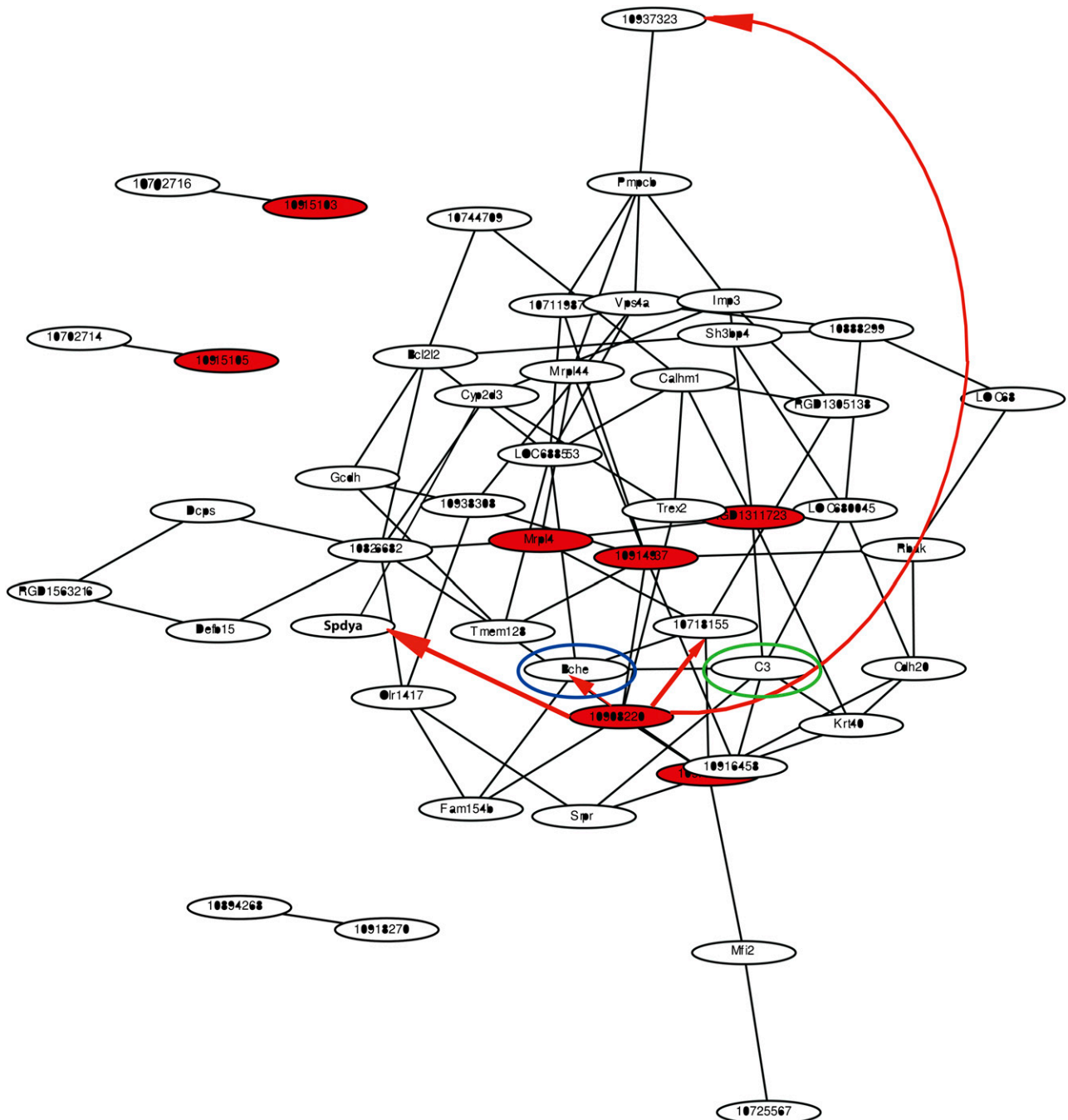


**FIGURE 6.** A gene expression network regulating C3 activation. eQTL mapping was performed by combining microarray expression data with genetic markers in an F<sub>2</sub>(DA × PVG) intercross. Strongly connected hub genes in eQTL gene expression networks were searched for using graphical Gaussian models leading to the identification of a network regulated by D8Rat56. The network includes 48 genes, including complement C3. The association between the genes in the network is based on pairwise covariation of expression levels, which is graphically depicted. *Cis*-regulated genes are marked with red circles and the red arrows link the *cis*-regulated transcript 10908220, a TF orthologous to FOXK2 (Ensembl gene ID ENSRNOG00000039894), with the transcripts in the cluster originating from genes with a known binding site for this TF, among them BChE (blue ring), which is positioned immediately upstream of C3 (green ring).

The genetic regulation of the complement cascade is complex, because the system is composed of multiple units distributed throughout the genome. A novel finding of this study is that of a marked co-regulated expression of several of the complement components with different members of the CLEC family, which suggests an intimate relationship between these two important parts of the innate immune system. The CLECs constitute a family of proteins that similar to complement mediates a wide range of

functions, including cell–cell adhesion, immune responses, and apoptosis (68, 69). Synergistic action between CLECs and complement components is known to occur, linking innate immune activation with systemic adaptive immune responses (69, 70). In the present study, we identify three different eQTL *trans*-regulating the expression of C1qa, C1qb, and C9, respectively, that all contain different *cis*-regulated CLECs. However, it was not possible to find any clear pairwise interconnectivity expression patterns of the transcripts

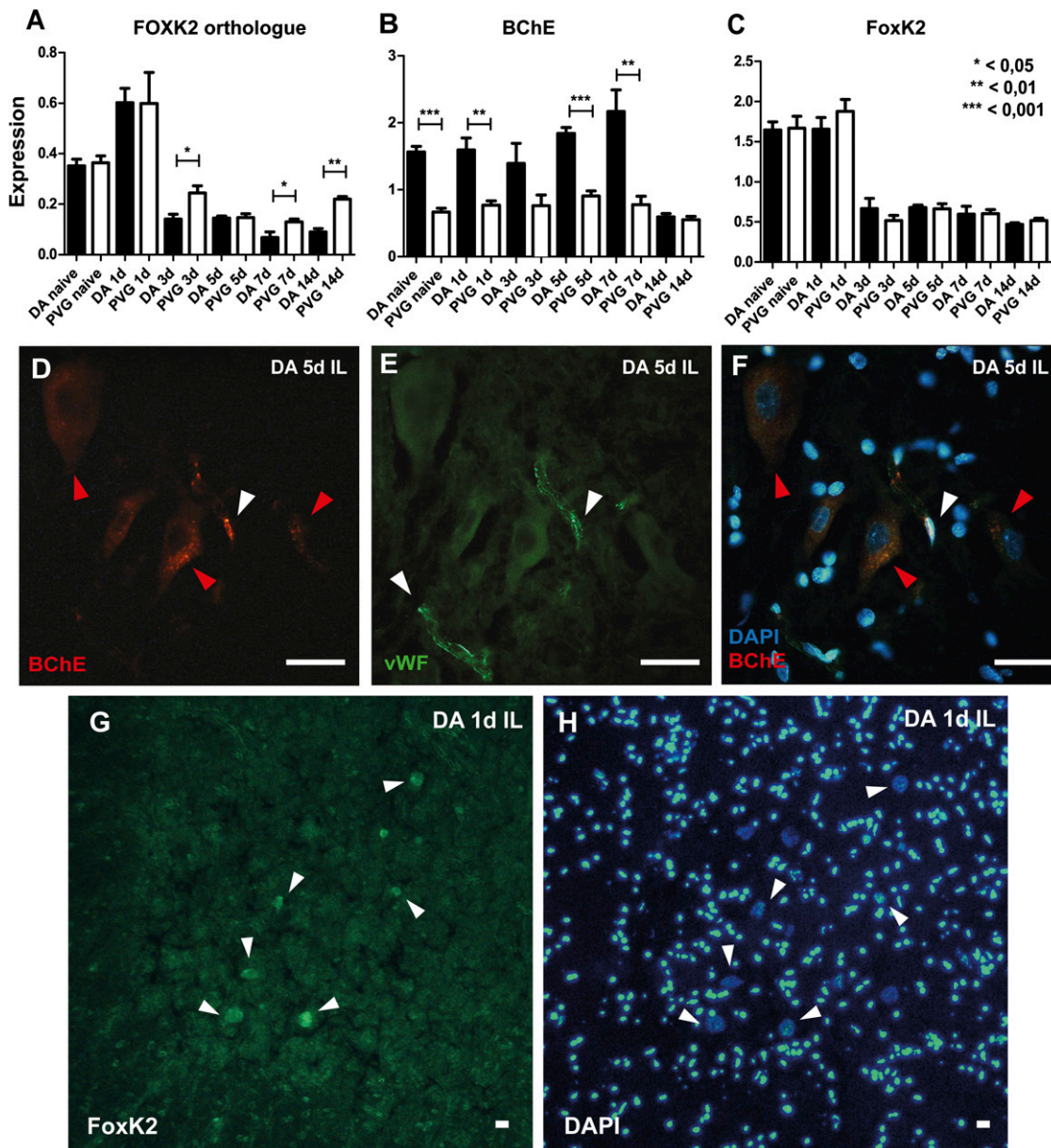


**FIGURE 7.** Expression of the FOXX2 orthologue, FoxK2, and BChE in DA and PVG rats after nerve injury. The FOXX2 orthologue, a potential master regulator of the C3 gene network, is upregulated early following injury, with subsequent downregulation to levels below those of naive animals. Expression is significantly lower in DA compared with PVG rats at 3, 7, and 14 d after VRA (**A**). The BChE gene contains a TF binding site for the FOXX2 orthologue, and expression is generally higher in DA than in PVG rats, with peak expression 7 d after ventral root avulsion, a time point when expression of the FOXX2 orthologue is most depressed in DA (**B**). The expression of the rat FoxK2 paralog is similar to the human FOXX2 orthologue, with downregulation after injury, but it lacks the initial upregulation as well as differences between the strains (**C**). BChE immunoreactivity is evident in the cytoplasm of motor neurons (**D**), but it can also be detected on vWF-positive blood vessels/endothelia (**E**). The spatial relationship between BChE, vWF, and nuclear DAPI staining is shown in (**F**) (motor neuron is indicated by a red arrow and blood vessels are indicated with white arrows in (D)–(F)). FoxK2 immunoreactivity is present in axotomized motor neurons (**G**; white arrowheads). The same section with nuclear DAPI staining, where motor neurons are easily recognized by their larger size, is shown in (**H**). Scale bars, 40  $\mu$ m.

within these three gene clusters. This pattern clearly differed from that of C3 regulation, which was not coregulated with any CLECs. Very little is known about any possible involvement of CLECs in the pathogenesis of neurodegenerative/inflammatory diseases. Notably, however, one of the first replicated non-HLA genes to be associated with the risk of multiple sclerosis is CLEC16A (71). The observation that C1qa and C1qb genes belong to different gene expression networks is interesting, as expression of different C1q subunits has been shown to be synchronized (72). However, a recent study, also investigating the role of C1q in the CNS in the setting of synaptic

physiology, illustrated that the expression of the three separate genes varied following the same stimulation, suggesting that the expression of the different subunits at least in some instances may vary (73). It can be speculated whether a separately controlled expression may be beneficial in some contexts, for example in case of Abs toward a specific C1q chain (74), because all three are necessary to form a fully functional C1q molecule (20). Thus, even though the existing literature indicates mechanisms that synchronize the expression of the different C1q components, our data suggest that this view should be modified, because unbiased gene expression mapping

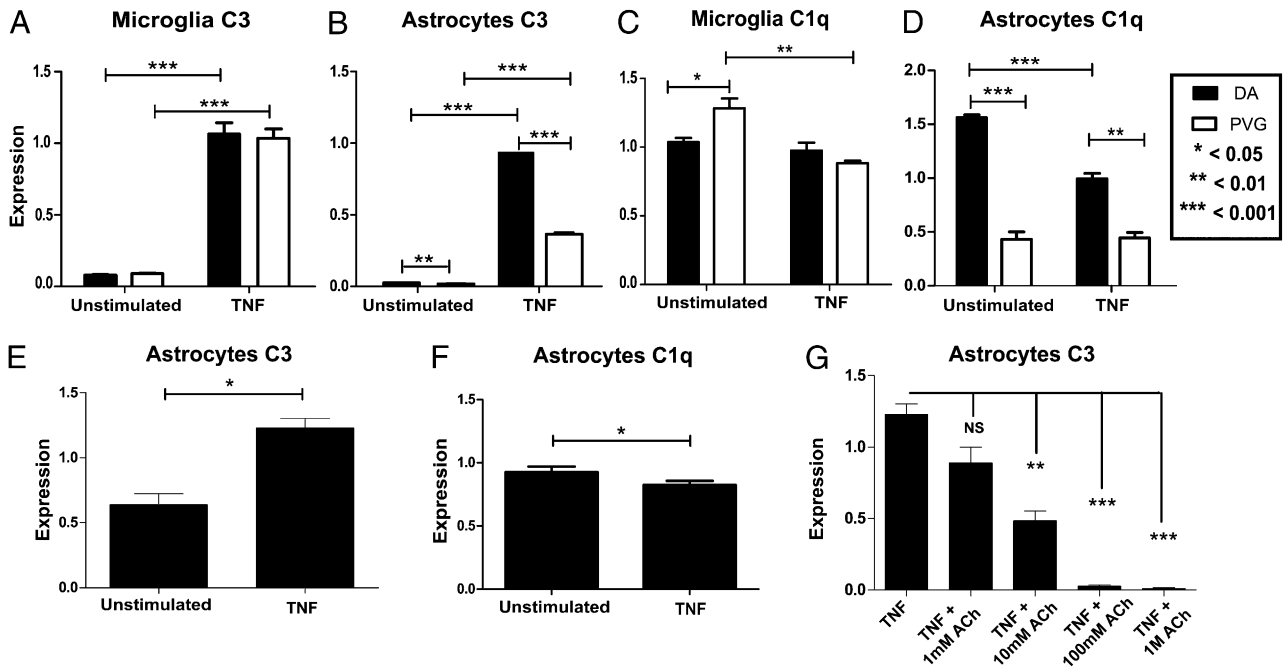


**FIGURE 8.** C3 expression is increased in microglia and astrocytes following TNF- $\alpha$  stimulation. Primary astrocyte and microglia cultures were established from adult DA and PVG rat brains and stimulated with TNF- $\alpha$  (20 ng/ml), which resulted in highly increased expression of C3 in both microglia (A) and astrocytes (B). In contrast, TNF- $\alpha$  did not have a discernible effect on C1q expression in either microglia (C) or astrocytes (D), supporting the notion of different pathways regulating C3 and C1q expression. A similar result was obtained also in mouse astrocytes, where C3 (E), but not C1q (F), expression was increased upon stimulation with TNF- $\alpha$ . ACh-abrogated TNF- $\alpha$  induced C3 expression in a dose-dependent manner (G).

clearly suggests that the different genes belong to separate expression networks.

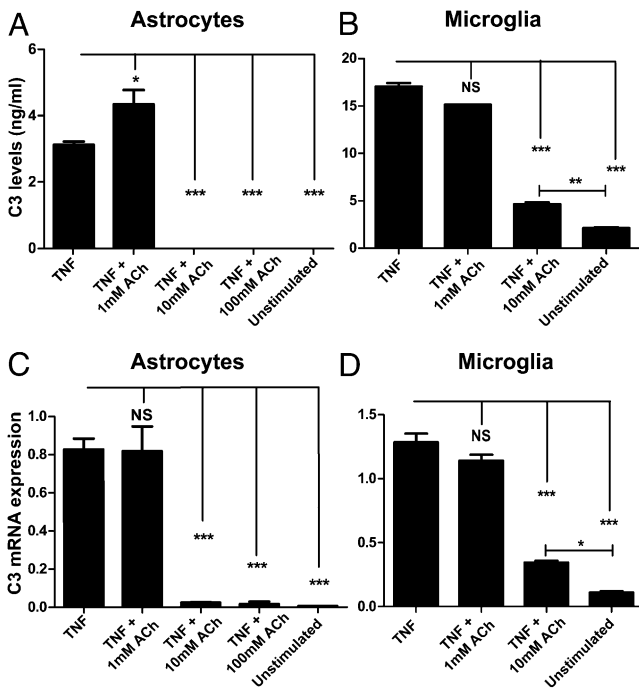


**FIGURE 9.** ACh attenuates TNF- $\alpha$ -induced upregulation of C3 in both astrocytes and microglia. To confirm the observed effect of ACh on TNF- $\alpha$ -induced C3 expression also on protein level, new primary astrocyte and microglia cultures were established from DA rats. C3 protein levels were quantified in supernatants using ELISA demonstrating a dose-dependent attenuation of TNF- $\alpha$ -induced C3 upregulation in both astrocytes (A) and microglia (B). C3 was detected in astrocyte cultures only after stimulation with TNF- $\alpha$  alone or with TNF- $\alpha$  in combination with the weakest ACh concentration (A). RT-PCR was performed on the cultured cells to determine C3 mRNA levels and demonstrated a pattern very similar to that of the protein levels (C, D).

In summary, in this study we dissected strain-dependent differences in expression of complement components in the CNS using a large-scale transcription profiling approach, where we found regulation of C9 and C1q subunits by gene regions containing different members of the CLEC family. We also identify a gene expression network regulated by a new putative transcription factor that includes BChE and C3. The link between BChE and C3 sheds new light on pathways regulating complement expression in the nervous system, and in turn of relevance for neuroinflammatory/degenerative diseases characterized by increased C3 expression.

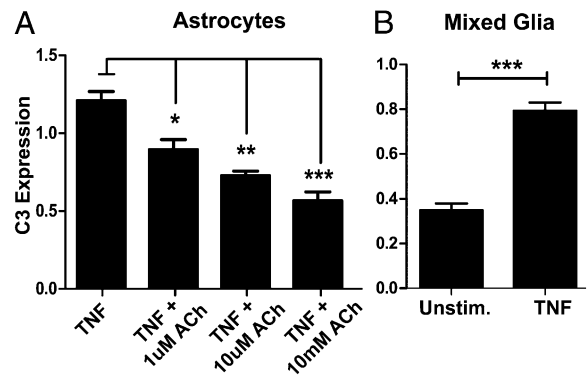


**FIGURE 10.** ACh attenuates C3 expression at low concentrations, when cholinesterase inhibitors are added. TNF- $\alpha$  induces C3 expression in mixed glia cultures. Astrocytes were extracted and the experiments repeated using the same medium and concentration of TNF- $\alpha$  (20 ng/ml), but this time in combination with lower concentrations of ACh (10 mM/10  $\mu$ M or 1  $\mu$ M, respectively), together with 0.6 mM cholinesterase inhibitor eserine hemisulfate to increase the stability of ACh. This confirmed the previously identified dose-dependent ACh-mediated attenuation of TNF- $\alpha$ -induced C3 expression (A). A mixed glia culture of astrocytes and microglia responded similarly as the individual populations following TNF- $\alpha$  stimulation, with upregulation of C3 (B).

## Acknowledgments

We thank Dr. Maja Jagodic for expert scientific advice, Karin Johnsson and Daan Hurkmans for valuable help with RT-PCRs, Nada Abdelmagid for help with tissue dissection, and Dr. Anna Hrabovska for providing the BChE Ab.

## Disclosures

The authors have no financial conflicts of interest.

## References

- Markiewski, M. M., and J. D. Lambris. 2007. The role of complement in inflammatory diseases from behind the scenes into the spotlight. *Am. J. Pathol.* 171: 715–727.
- Ricklin, D., G. Hajishengallis, K. Yang, and J. D. Lambris. 2010. Complement: a key system for immune surveillance and homeostasis. *Nat. Immunol.* 11: 785–797.
- Zipfel, P. F., and C. Skerka. 2009. Complement regulators and inhibitory proteins. *Nat. Rev. Immunol.* 9: 729–740.
- Gasque, P. 2004. Complement: a unique innate immune sensor for danger signals. *Mol. Immunol.* 41: 1089–1098.
- Dunkelberger, J. R., and W. C. Song. 2010. Complement and its role in innate and adaptive immune responses. *Cell Res.* 20: 34–50.
- Carroll, M. C. 2004. The complement system in regulation of adaptive immunity. *Nat. Immunol.* 5: 981–986.
- Sjöberg, A. P., L. A. Trouw, and A. M. Blom. 2009. Complement activation and inhibition: a delicate balance. *Trends Immunol.* 30: 83–90.
- Bellander, B. M., S. K. Singhrao, M. Ohlsson, P. Mattsson, and M. Svensson. 2001. Complement activation in the human brain after traumatic head injury. *J. Neurotrauma* 18: 1295–1311.
- Székely, G., R. Szegei, K. Hirschberg, T. Gombos, L. Varga, I. Karádi, L. Entz, Z. Székely, P. Garred, Z. Prohászka, and G. Füst. 2009. Strong complement activation after acute ischemic stroke is associated with unfavorable outcomes. *Atherosclerosis* 204: 315–320.
- Fonseca, M. I., J. Zhou, M. Botto, and A. J. Tenner. 2004. Absence of C1q leads to less neuropathology in transgenic mouse models of Alzheimer's disease. *J. Neurosci.* 24: 6457–6465.
- Lambert, J. C., S. Heath, G. Even, D. Campion, K. Sleegers, M. Hiltunen, O. Combarros, D. Zelenika, M. J. Bullido, B. Tavernier, et al; European Alzheimer's Disease Initiative Investigators. 2009. Genome-wide association study identifies variants at CLU and CR1 associated with Alzheimer's disease. *Nat. Genet.* 41: 1094–1099.
- Bonifati, D. M., and U. Kishore. 2007. Role of complement in neurodegeneration and neuroinflammation. *Mol. Immunol.* 44: 999–1010.
- Wang, Y., A. M. Hancock, J. Bradner, K. A. Chung, J. F. Quinn, E. R. Peskind, D. Galasko, J. Jankovic, C. P. Zabetian, H. M. Kim, et al. 2011. Complement 3 and factor H in human cerebrospinal fluid in Parkinson's disease, Alzheimer's disease, and multiple-system atrophy. *Am. J. Pathol.* 178: 1509–1516.
- Swanberg, M., K. Duvefelt, M. Diez, J. Hillert, T. Olsson, F. Piehl, and O. Lidman. 2006. Genetically determined susceptibility to neurodegeneration is associated with expression of inflammatory genes. *Neurobiol. Dis.* 24: 67–88.
- Lidman, O., M. Swanberg, L. Horvath, K. W. Broman, T. Olsson, and F. Piehl. 2003. Discrete gene loci regulate neurodegeneration, lymphocyte infiltration, and major histocompatibility complex class II expression in the CNS. *J. Neurosci.* 23: 9817–9823.
- Al Nimer, F., A. D. Beyeen, R. Lindblom, M. Ström, S. Aeinehband, O. Lidman, and F. Piehl. 2011. Both MHC and non-MHC genes regulate inflammation and T-cell response after traumatic brain injury. *Brain Behav. Immun.* 25: 981–990.
- Laird, P. W., A. Zijderveld, K. Linders, M. A. Rudnicki, R. Jaenisch, and A. Berns. 1991. Simplified mammalian DNA isolation procedure. *Nucleic Acids Res.* 19: 4293.
- Darvasi, A., and M. Soller. 1994. Optimum spacing of genetic markers for determining linkage between marker loci and quantitative trait loci. *Theor. Appl. Genet.* 89: 351–357.
- Jacob, H. J., D. M. Brown, R. K. Bunker, M. J. Daly, V. J. Dzau, A. Goodman, G. Koike, V. Kren, T. Kurtz, A. Lernmark, et al. 1995. A genetic linkage map of the laboratory rat, *Rattus norvegicus*. *Nat. Genet.* 9: 63–69.
- Kishore, U., C. Gaboriaud, P. Waters, A. K. Shrive, T. J. Greenough, K. B. Reid, R. B. Sim, and G. J. Arlaud. 2004. C1q and tumor necrosis factor superfamily: modularity and versatility. *Trends Immunol.* 25: 551–561.
- Hrabovska, A., V. Bernard, and E. Krejci. 2010. A novel system for the efficient generation of antibodies following immunization of unique knockout mouse strains. *PLoS ONE* 5: e12892.
- Dagerlind, A., K. Friberg, A. J. Bean, and T. Hökfelt. 1992. Sensitive mRNA detection using unfixed tissue: combined radioactive and non-radioactive in situ hybridization histochemistry. *Histochemistry* 98: 39–49.
- de Bruijn, M. H., and G. H. Fey. 1985. Human complement component C3: cDNA coding sequence and derived primary structure. *Proc. Natl. Acad. Sci. USA* 82: 708–712.
- Strom, M., F. Al Nimer, R. Lindblom, J. R. Nyengaard, and F. Piehl. 2012. Naturally occurring genetic variability in expression of *Gsta4* is associated with differential survival of axotomized rat motoneurons. *Neuromolecular Med.* 14: 15–29.
- Irizarry, R. A., B. Hobbs, F. Collin, Y. D. Beazer-Barclay, K. J. Antonellis, U. Scherf, and T. P. Speed. 2003. Exploration, normalization, and summaries of high density oligonucleotide array probe level data. *Biostatistics* 4: 249–264.
- Wang, J., R. W. Williams, and K. F. Manly. 2003. WebQTL: Web-based complex trait analysis. *Neuroinformatics* 1: 299–308.
- Falcon, S., and R. Gentleman. 2007. Using GOstats to test gene lists for GO term association. *Bioinformatics* 23: 257–258.
- Schäfer, J., and K. Strimmer. 2005. An empirical Bayes approach to inferring large-scale gene association networks. *Bioinformatics* 21: 754–764.
- Heinig, M., E. Petretto, C. Wallace, L. Bottolo, M. Rotival, H. Lu, Y. Li, R. Sarwar, S. R. Langley, A. Bauerfeind, et al; Cardiogenics Consortium. 2010. A trans-acting locus regulates an anti-viral expression network and type 1 diabetes risk. *Nature* 467: 460–464.
- Roider, H. G., A. Kanhere, T. Manke, and M. Vingron. 2007. Predicting transcription factor affinities to DNA from a biophysical model. *Bioinformatics* 23: 134–141.
- Manke, T., H. G. Roider, and M. Vingron. 2008. Statistical modeling of transcription factor binding affinities predicts regulatory interactions. *PLoS Comput. Biol.* 4: e1000039.
- Roider, H. G., T. Manke, S. O'Keefe, M. Vingron, and S. A. Haas. 2009. PASTAA: identifying transcription factors associated with sets of co-regulated genes. *Bioinformatics* 25: 435–442.
- Weitnauer, E., A. Robitzki, and P. G. Layer. 1998. Aryl acylamidase activity exhibited by butyrylcholinesterase is higher in chick than in horse, but much lower than in fetal calf serum. *Neurosci. Lett.* 254: 153–156.
- Vijayaraghavan, S., A. Karami, S. Aeinehband, H. Behbahani, A. Grandien, B. Nilsson, K. N. Ekdahl, R. P. Lindblom, F. Piehl, and T. Darreh-Shori. 2013. Regulated extracellular choline acetyltransferase activity: the plausible missing link of the distant action of acetylcholine in the cholinergic anti-inflammatory pathway. *PLoS ONE* 8: e65936.
- Lundberg, C., O. Lidman, R. Holmdahl, T. Olsson, and F. Piehl. 2001. Neurodegeneration and glial activation patterns after mechanical nerve injury are differentially regulated by non-MHC genes in congenic inbred rat strains. *J. Comp. Neurol.* 431: 75–87.
- Stahel, P. F., M. A. Flierl, B. P. Morgan, I. Persigehl, C. Stoll, C. Conrad, B. M. Touban, W. R. Smith, K. Beauchamp, O. I. Schmidt, et al. 2009. Absence of the complement regulatory molecule CD59a leads to exacerbated neuropathology after traumatic brain injury in mice. *J. Neuroinflammation* 6: 2.
- Nimer, F. A., R. Lindblom, M. Strom, A. O. Guerreiro-Cacais, R. Parsa, S. Aeinehband, T. Mathiesen, O. Lidman, and F. Piehl. 2013. Strain influences on inflammatory pathway activation, cell infiltration and complement cascade after traumatic brain injury in the rat. *Brain Behav. Immun.* 27: 109–122.
- Stevens, B., N. J. Allen, L. E. Vazquez, G. R. Howell, K. S. Christopherson, N. Nouri, K. D. Micheva, A. K. Mehalow, A. D. Huberman, B. Stafford, et al. 2007. The classical complement cascade mediates CNS synapse elimination. *Cell* 131: 1164–1178.
- Swanberg, M., O. Lidman, L. Padyukov, P. Eriksson, E. Akesson, M. Jagodic, A. Lobell, M. Khademi, O. Börjesson, C. M. Lindgren, et al. 2005. *MHC2TA* is associated with differential MHC molecule expression and susceptibility to rheumatoid arthritis, multiple sclerosis and myocardial infarction. *Nat. Genet.* 37: 486–494.
- Hubner, N., C. A. Wallace, H. Zimdahl, E. Petretto, H. Schulz, F. Maciver, M. Mueller, O. Hummel, J. Monti, V. Zidek, et al. 2005. Integrated transcriptional profiling and linkage analysis for identification of genes underlying disease. *Nat. Genet.* 37: 243–253.
- Ghazalpour, A., S. Doss, B. Zhang, S. Wang, C. Plaisier, R. Castellanos, A. Brozell, E. E. Schadt, T. A. Drake, A. J. Lusis, and S. Horvath. 2006. Integrating genetic and network analysis to characterize genes related to mouse weight. *PLoS Genet.* 2: e130.
- Salamone, G., G. Lombardi, S. Gori, K. Nahmod, C. Jancic, M. M. Amaral, M. Vermeulen, A. Español, M. E. Sales, and J. Geffner. 2011. Cholinergic modulation of dendritic cell function. *J. Neuroimmunol.* 236: 47–56.
- Rosas-Ballina, M., P. S. Olofsson, M. Ochani, S. I. Valdés-Ferrer, Y. A. Levine, C. Reardon, M. W. Tusche, V. A. Pavlov, U. Andersson, S. Chavan, et al. 2011. Acetylcholine-synthesizing T cells relay neural signals in a vagus nerve circuit. *Science* 334: 98–101.
- Nguyen, H. X., M. D. Galvan, and A. J. Anderson. 2008. Characterization of early and terminal complement proteins associated with polymorphonuclear leukocytes in vitro and in vivo after spinal cord injury. *J. Neuroinflammation* 5: 26.
- Darvesh, S., D. A. Hopkins, and C. Geula. 2003. Neurobiology of butyrylcholinesterase. *Nat. Rev. Neurosci.* 4: 131–138.
- Tracey, K. J. 2009. Reflex control of immunity. *Nat. Rev. Immunol.* 9: 418–428.
- Shi, F. D., W. H. Piao, Y. P. Kuo, D. I. Campagnolo, T. L. Vollmer, and R. J. Lukas. 2009. Nicotinic attenuation of central nervous system inflammation and autoimmunity. *J. Immunol.* 182: 1730–1739.
- Mesulam, M. M., and C. Geula. 1994. Butyrylcholinesterase reactivity differentiates the amyloid plaques of aging from those of dementia. *Ann. Neurol.* 36: 722–727.
- Terry, R. D., E. Masliah, D. P. Salmon, N. Butters, R. DeTeresa, R. Hill, L. A. Hansen, and R. Katzman. 1991. Physical basis of cognitive alterations in Alzheimer's disease: synapse loss is the major correlate of cognitive impairment. *Ann. Neurol.* 30: 572–580.
- Darvesh, S., A. M. Leblanc, I. R. Macdonald, G. A. Reid, V. Bhan, R. J. Macaulay, and J. D. Fisk. 2010. Butyrylcholinesterase activity in multiple sclerosis neuropathology. *Chem. Biol. Interact.* 187: 425–431.

51. Mis, K., T. Mars, M. Jevsek, M. Brank, K. Zajc-Kreft, and Z. Grubic. 2003. Localization of mRNAs encoding acetylcholinesterase and butyrylcholinesterase in the rat spinal cord by nonradioactive in situ hybridization. *J. Histochem. Cytochem.* 51: 1633–1644.
52. Darreh-Shori, T., S. Vijayaraghavan, S. Aeinehband, F. Piehl, R. P. Lindblom, B. Nilsson, K. N. Ekdahl, B. Långström, O. Almkvist, and A. Nordberg. 2013. Functional variability in butyrylcholinesterase activity regulates intrathecal cytokine and astroglial biomarker profiles in patients with Alzheimer's disease. *Neurobiol. Aging* 34: 2465–2481.
53. McAlpine, F. E., and M. G. Tansey. 2008. Neuroinflammation and tumor necrosis factor signaling in the pathophysiology of Alzheimer's disease. *J. Inflamm. Res.* 1: 29–39.
54. Stellwagen, D., and R. C. Malenka. 2006. Synaptic scaling mediated by glial TNF- $\alpha$ . *Nature* 440: 1054–1059.
55. Centonze, D., L. Muzio, S. Rossi, F. Cavalinini, V. De Chiara, A. Bergami, A. Musella, M. D'Amelio, V. Cavallucci, A. Martorana, et al. 2009. Inflammation triggers synaptic alteration and degeneration in experimental autoimmune encephalomyelitis. *J. Neurosci.* 29: 3442–3452.
56. Shytle, R. D., T. Mori, K. Townsend, M. Vendrame, N. Sun, J. Zeng, J. Ehrhart, A. A. Silver, P. R. Sanberg, and J. Tan. 2004. Cholinergic modulation of microglial activation by  $\alpha 7$  nicotinic receptors. *J. Neurochem.* 89: 337–343.
57. McCaman, R. E., D. Weinreich, and H. Borys. 1973. Endogenous levels of acetylcholine and choline in individual neurons of *Aplysia*. *J. Neurochem.* 21: 473–476.
58. Bazelyansky, M., E. Robey, and J. F. Kirsch. 1986. Fractional diffusion-limited component of reactions catalyzed by acetylcholinesterase. *Biochemistry* 25: 125–130.
59. Greig, N. H., T. Utsuki, Q. Yu, X. Zhu, H. W. Holloway, T. Perry, B. Lee, D. K. Ingram, and D. K. Lahiri. 2001. A new therapeutic target in Alzheimer's disease treatment: attention to butyrylcholinesterase. *Curr. Med. Res. Opin.* 17: 159–165.
60. Cuadra, G., K. Summers, and E. Giacobini. 1994. Cholinesterase inhibitor effects on neurotransmitters in rat cortex in vivo. *J. Pharmacol. Exp. Ther.* 270: 277–284.
61. Farar, V., F. Mohr, M. Legrand, B. Lamotte d'Incamps, J. Cendelin, J. Leroy, M. Abitbol, V. Bernard, F. Baud, V. Fournet, et al. 2012. Near-complete adaptation of the PRiMA knockout to the lack of central acetylcholinesterase. *J. Neurochem.* 122: 1065–1080.
62. Hannehalli, S., and K. H. Kaestner. 2009. The evolution of Fox genes and their role in development and disease. *Nat. Rev. Genet.* 10: 233–240.
63. Jonsson, H., and S. L. Peng. 2005. Forkhead transcription factors in immunology. *Cell. Mol. Life Sci.* 62: 397–409.
64. Long, S. A., and J. H. Buckner. 2011. CD4<sup>+</sup>FOXP3<sup>+</sup> T regulatory cells in human autoimmunity: more than a numbers game. *J. Immunol.* 187: 2061–2066.
65. Wijchers, P. J., M. F. Hoekman, J. P. Burbach, and M. P. Smidt. 2006. Identification of forkhead transcription factors in cortical and dopaminergic areas of the adult murine brain. *Brain Res.* 1068: 23–33.
66. Li, C., C. F. Lai, D. S. Sigman, and R. B. Gaynor. 1991. Cloning of a cellular factor, interleukin binding factor, that binds to NFAT-like motifs in the human immunodeficiency virus long terminal repeat. *Proc. Natl. Acad. Sci. USA* 88: 7739–7743.
67. Nirula, A., D. J. Moore, and R. B. Gaynor. 1997. Constitutive binding of the transcription factor interleukin-2 (IL-2) enhancer binding factor to the IL-2 promoter. *J. Biol. Chem.* 272: 7736–7745.
68. Takeuchi, O., and S. Akira. 2010. Pattern recognition receptors and inflammation. *Cell* 140: 805–820.
69. Areschoug, T., and S. Gordon. 2008. Pattern recognition receptors and their role in innate immunity: focus on microbial protein ligands. *Contrib. Microbiol.* 15: 45–60.
70. Figdor, C. G., and A. B. van Spriel. 2010. Fungal pattern-recognition receptors and tetraspanins: partners on antigen-presenting cells. *Trends Immunol.* 31: 91–96.
71. Hoppenbrouwers, I. A., Y. S. Aulchenko, A. C. Janssens, S. V. Ramagopalan, L. Broer, M. Kayser, G. C. Ebers, B. A. Oostra, C. M. van Duijn, and R. Q. Hintzen. 2009. Replication of CD58 and CLEC16A as genome-wide significant risk genes for multiple sclerosis. *J. Hum. Genet.* 54: 676–680.
72. Chen, G., C. S. Tan, B. K. Teh, and J. Lu. 2011. Molecular mechanisms for synchronized transcription of three complement C1q subunit genes in dendritic cells and macrophages. *J. Biol. Chem.* 286: 34941–34950.
73. Bialas, A. R., and B. Stevens. 2013. TGF- $\beta$  signaling regulates neuronal C1q expression and developmental synaptic refinement. *Nat. Neurosci.* 16: 1773–1782.
74. Radanova, M., V. Vasilev, B. Deliyska, U. Kishore, V. Ikonov, and D. Ivanova. 2012. Anti-C1q autoantibodies specific against the globular domain of the C1qB-chain from patient with lupus nephritis inhibit C1q binding to IgG and CRP. *Immunobiology* 217: 684–691.